Journal of Power Sources 194 (2009) 146–160

Contents lists available at ScienceDirect

Journal of Power Sources

journal homepage: www.elsevier.com/locate/jpowsour

Review

Gas diffusion layer for proton exchange membrane fuel cells—A review

L. Cindrella[a,b], A.M. Kannan[a,*], J.F. Lin[a], K. Saminathan[a], Y. Ho[c], C.W. Lin[d], J. Wertz[e]

[a] Fuel Cell Research Laboratory, Department of Engineering Technology, Arizona State University, Mesa, AZ 85212, USA
[b] Department of Chemistry, National Institute of Technology, Tiruchirappalli 620015, India
[c] Department of Biotechnology, College of Health Science, Asia University, Taichung 41354, Taiwan
[d] Department of Chemical Engineering, National Yunlin University of Science and Technology, Yunlin 640, Taiwan
[e] Hollingsworth & Vose Co., A.K. Nicholson Research Lab, 219 Townsend Road, West Groton, MA 01472, USA

ARTICLE INFO

Article history:
Received 6 February 2009
Received in revised form 30 March 2009
Accepted 9 April 2009
Available online 18 April 2009

Keywords:
Gas diffusion layer
Hydrophobicity
Porosity
Water management
Gas permeability
Proton exchange membrane fuel cell

ABSTRACT

Gas diffusion layer (GDL) is one of the critical components acting both as the functional as well as the support structure for membrane–electrode assembly in the proton exchange membrane fuel cell (PEMFC). The role of the GDL is very significant in the H_2/air PEM fuel cell to make it commercially viable. A bibliometric analysis of the publications on the GDLs since 1992 shows a total of 400+ publications (>140 papers in the Journal of Power Sources alone) and reveals an exponential growth due to reasons that PEMFC promises a lot of potential as the future energy source for varied applications and hence its vital component GDL requires due innovative analysis and research. This paper is an attempt to pool together the published work on the GDLs and also to review the essential properties of the GDLs, the method of achieving each one of them, their characterization and the current status and future directions. The optimization of the functional properties of the GDLs is possible only by understanding the role of its key parameters such as structure, porosity, hydrophobicity, hydrophilicity, gas permeability, transport properties, water management and the surface morphology. This paper discusses them in detail to provide an insight into the structural parts that make the GDLs and also the processes that occur in the GDLs under service conditions and the characteristic properties. The required balance in the properties of the GDLs to facilitate the counter current flow of the gas and water is highlighted through its characteristics.

Contents

1. Introduction 146
2. Characteristics of GDL 147
 2.1. Hydrophobicity and hydrophilicity 147
 2.2. Porosity 148
 2.3. Permeability 149
 2.4. Transport properties 149
 2.5. Electron transport 152
 2.6. Compression 155
 2.7. Structure 155
3. Fuel cell performance 156
4. Coating processes 157
5. Manufacture 157
6. Conclusion 157
 References 157

1. Introduction

The proton exchange membrane fuel cells (PEMFCs) are the promising power sources for automotive, stationary and portable equipments because of their higher power densities and

* Corresponding author. Tel.: +1 480 727 1102; fax: +1 480 727 1723.
E-mail address: amk@asu.edu (A.M. Kannan).

0378-7753/$ – see front matter © 2009 Elsevier B.V. All rights reserved.
doi:10.1016/j.jpowsour.2009.04.005

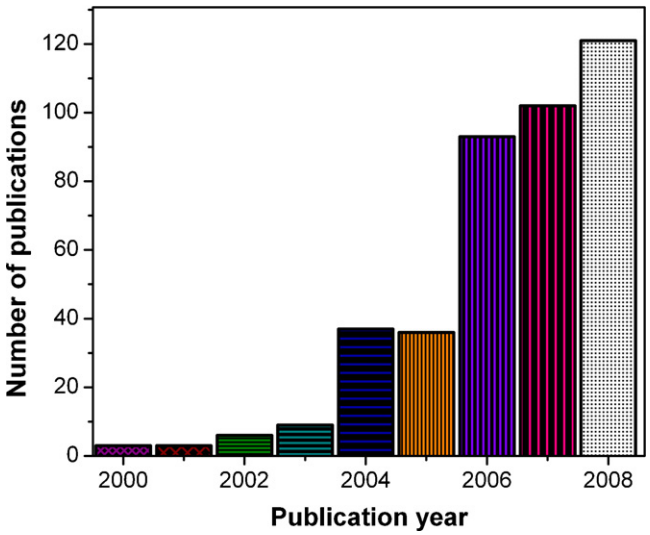

Fig. 1. Bibliometric analysis of the publications.

environmental benefits and hence they have attracted enormous R&D attention during the last decade. The crucial part of the fuel cell system is the membrane–electrode assembly (MEA) which consists of a proton exchange membrane with a layer of catalyst on both sides and a gas diffusion layer (GDL) in contact with each of the catalyst layers. The commercial success of the PEMFCs rests with their ability to show optimal performance with H_2/air system at high current density. However, when air is used as oxidant, the power density values are reduced due to mass transport limitations primarily at the cathode. GDL is one of the critical components of a fuel cell that has the ability to influence the H_2/air system as its basic functions are transportation of the reactant gas from flow channels to catalyst layer effectively, draining out liquid water from catalyst layer to flow channels, conducting electrons with low resistance and keeping the membrane in wet condition at low humidity. Understanding the functionality of GDL is very essential for its optimization to meet the service conditions. A bibliometric analysis of the publications on GDL since 1992 has been carried out. The data were based on the online version of the Science Citation Index (SCI), Web of Science. SCI is a multidisciplinary database of the Institute for Scientific Information (ISI), Philadelphia, USA. According to Journal Citation Reports (JCR), it indexed 6426 major journals with citation references across 172 scientific disciplines in 2007. "Gas Diffusion Layer" and ("fuel cell" or "fuel cells") were used as keywords to search titles, abstracts, or keywords. The number of publications in the past 5 years (Fig. 1) reveals that the significant and indispensable role of the GDL has triggered systematic and scientific analysis sprawling over the areas of interdisciplinary science. In addition, there are also several patents and book chapters. It is worth mentioning about the book chapters describing the materials properties, characterization and fuel cell performance of the GDLs [1–3]. This paper focuses on the review of the methods of preparation of GDL, its structure and characterization along with the recent developments and future directions.

2. Characteristics of GDL

The power performance of the PEMFC is strongly influenced by interdependent properties such as water management, porosity and graded structure of GDL. The GDL should possess the combined and balanced properties of hydrophobicity (water expelling) and hydrophilicity (water retaining). These properties have to be balanced carefully to ensure that the fuel cell system works without flooding and high humidity. The pore dimension and the surface

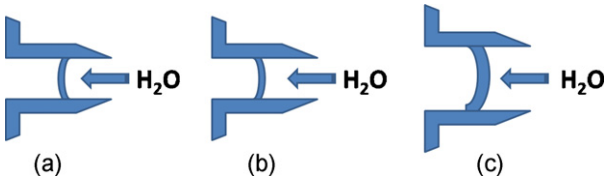

Fig. 2. Structure of (a) hydrophilic, (b) small hydrophobic and (c) larger hydrophobic GDL pores showing water transport.

feature of the droplet affect the flow of water droplets. Fig. 2 explains the effect of expanded and contracted pores in water transport: water flows easily in contact with a hydrophilic and concave pore (a), whereas its flow in a same sized hydrophobic convex pore (b) is constrained and requires a larger sized pore (c). The ideal GDLs should have properties such as good gas diffusion [4,5] with optimum bending stiffness, porosity, surface contact angle, air permeability, water vapor diffusion, electrical/electronic conductivity, crack free surface morphology, high mechanical integrity and enhanced oxidative stability along with durability at various operating conditions including freezing.

2.1. Hydrophobicity and hydrophilicity

Numerous research papers aim at developing GDLs with improved efficiency based on theoretical and experimental analysis. Lim and Wang [6] have studied the effects of hydrophobic fluorinated ethylene propylene content in GDL and inferred the crucial role of hydrophobic content on the surface morphology of the GDL and hence on the performance of the PEM fuel cell. Park et al. [7] have investigated the water management in the micro-layer (ML) and the gas diffusion medium (GDM) as the function of the hydrophobic content of the GDM and inferred that the capillary-force-driven water movement and the shear-force- or vaporization-driven water transportation should be considered and balanced for both the ML and the GDM structures. Lin and Nguyen [8] observed that adding polytetrafluoroethylene (PTFE) to the GDL could enhance gas transport and water transport when a cell operates under flooding condition, but excessive PTFE loading could lead to a high flooding level in the catalyst layer. The hydrophobic treatment and larger air permeability of a GDL substrate were found to improve the start-up performance of a PEMFC [9]. A study by Park et al. [10] indicated that the optimized PTFE content of GDL resulted in an effective water management and improved oxygen diffusion kinetics in the membrane–electrode assembly. Wang et al. [11] have reported sucrose carbonization of GDL in order to obtain high hydrophobicity with low PTFE loading. Gostick et al. [12] measured capillary pressure curves for both the total pore network and the pore network consisting of only hydrophilic pores of GDL, which enabled the determination of capillary pressure curves to infer on GDL flooding. Jordan et al. [13] analyzed the effect of hydrophobicity and porosity of the diffusion layer on water impregnation and gas diffusion through the GDL and the influence of the diffusion layer morphology on cell performance. The effects of porosity, thickness and wettability of a micro-porous layer on the two-phase transport in PEFC were studied by Pasaogullari and Wang [14]. Lee et al. [15] evaluated the effect of thickness of the GDL on the performance of the PEM fuel cell. Very recently, Kannan et al. [16] have reported the development of GDLs by in situ growth of multi-walled carbon nanotubes as micro-porous layer on carbon paper substrates. As this micro-porous layer does not have any hydrophobic agent, the fuel cell performance is reported to be stable even at 50% RH conditions.

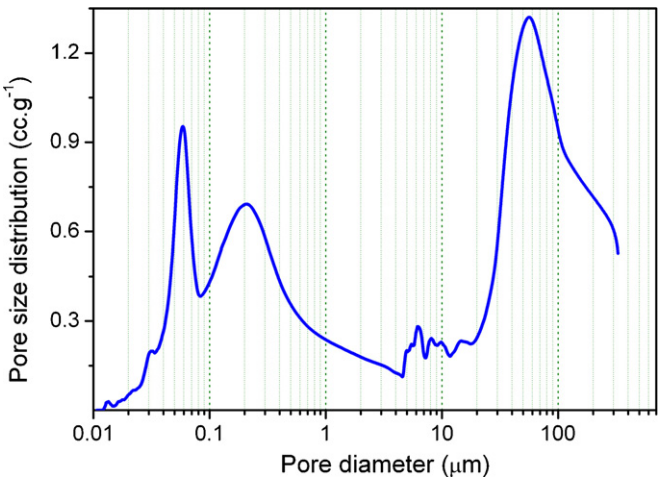

Fig. 3. Pore size distribution of a typical GDL fabricated with Pureblack carbon based micro-porous layer.

2.2. Porosity

GDLs are typically multi-layered carbon based porous materials containing a macro-porous substrate or backing which provides mechanical strength, electrical conductivity and mass transport for the gas reactants and water product, and at least one micro-porous layer which enhances the electrical conductivity and improves the water management. As the macro-porous substrates for GDLs are either carbon cloth or non-woven carbon materials, the pore sizes of common macro-porous substrates (1–100 μm) are much larger than the average pore size of catalyst layers (a few hundred nanometers).

The two methods used to determine the bulk porosity of GDL are Mercury porosimetry and immersion method. Bulk porosity of a GDL is defined as its total pore volume divided by the summation of its total pore volume and its solid volume [17]. Bulk porosity is expected to affect the effective diffusion coefficient (D_{eff}) of a porous medium according to the following equation

$$D_{eff} = \frac{\varepsilon}{\tau D} \quad (1)$$

where ε is the porosity, τ is the tortuosity, and D is the binary diffusion coefficient of oxygen in nitrogen.

A mercury pore size analyzer estimates the total pore volume by measuring the amount of mercury penetrated into pores of a porous media as a function of the applied pressure. Pressure required to penetrate mercury into a certain size of pore is a function of the pore diameter. A Quantachrome PoreMaster-33 is a useful tool to analyze any porous media with pore sizes ranging between 3 nm and 300 μm. This tool can collect pore size distribution of all GDLs and bare macro-porous substrate. Pore size distribution of a typical GDL seen in Fig. 3 shows micro-, meso- and macro-pores of 0.06, 0.2 and 55 μm diameter, respectively. On the other hand, the immersion method weighs the sample before and after immersing in a wetting liquid to determine the bulk porosity. Williams et al. [17] determined the porosity of the different GDLs by the mercury porosimetry and the immersion method and reported that both methods have good agreement for all samples of GDL studied.

Porosity of the GDL allows the reactant gases to reach the reaction zones and the product water move out. In terms of water management, the role of the micro-porous layer of the cathode GDL is to effectively remove the product water so that the gaseous oxygen molecules can reach the reactions sites through the relatively dry pores [18]. The other functions are better ohmic behavior and also to facilitate optimum catalyst utilization. All these functions are exhibited by the controlled porosity of the GDL. The effects of the cross-section of the channel of the anode flow distributor and the porosity of the gas-diffusion layer on the transport phenomena have been simulated by Yan et al. [19]. The power density of 0.91 W cm^{-2} was reported by the micro-porous layer (MPL) containing 10 wt.% Black Pearls 2000 in composite carbon black, characterized with effective bi-functional pore structure [20]. Roshandel et al. [21] determined the porosity variation in the GDL as a function of the applied pressure and the amount of the water generated in the cell and inferred that when the electrical current density is low, the porosity variation in gas diffusion layer has no significant influence on the level of polarization whereas at higher current density the influence is very significant. The porosity variation causes non-uniformity in the mass transport which in turn reduces the current density and a lower fuel cell performance. A high efficiency bi-functional MPL with composite carbon black consisting of 20 wt.% Black Pearls 2000 carbon and 80 wt.% Acetylene Black carbon has been proposed by Wang et al. [22] to enhance the transportation of both reactant gases and liquid water. A study of the liquid water flux through differently structured GDL by Zhan et al. [23] has reported that GDL with a gradient of porosity and also with larger gradient is more favorable for liquid water discharge from catalyst layer into the gas channel. A pore network model of the GDL proposed by Gostick et al. [24] with a regular cubic network of pore bodies and pore throats following respective size distributions suggest that a dry GDL does not limit the performance of a PEMFC, but it may become a significant source of concentration polarization as the GDL becomes increasingly saturated with water.

The evaluation of carbon loading in the micro-porous layer by ac-impedance study indicated that the optimized micro-porous layer results in an effective water management thereby improving the oxygen diffusion kinetics [25]. The effect of porosity-graded micro-porous layer (GMPL) prepared by it with different content of NH_4Cl pore-former and decreasing the porosity of the GMPL from the inner layer at the membrane/MPL interface to the outer layer of the MPLs at the gas diffusion electrode/MPL interface. The performance of the PEMFCs has been studied and inferred that the micro-porous layer with graded porosity is beneficial for the electrode reactions of fuel cell reaction by facilitating the liquid water transportation through large pores and gas diffusion via small pores in the GMPLs [26]. Zhan et al. [27] analyzed the distribution of liquid water phase saturation for GDL structures such as GDL with uniform porosity, sudden change in porosity and with graded porosity. The effect of porosity changes on gas diffusion and liquid saturation due to water remaining in GDL pores has been calculated which indicated that for uniform porosity GDL, the gas diffusion increased with the increase of porosity and contact angle and decrease of the thickness of GDL. Atiyeh et al. [28] evaluated the net water drag coefficient at three current densities (0.3, 0.5 and 0.7 A cm^{-2}) for two combinations of anode/cathode relative humidity (60/100% and 100/60%) and stoichiometric ratios of H_2/air (1.4/3 and 1.4/2) and showed that the presence of MPL improved the cell performance although it did not affect the net water drag coefficient. Functionally graded nano-porous layers were designed by Kannan et al. [29] by combining carbon nanofibers with nano-chain type Pureblack carbon in the *z*-direction towards the catalyst layer and Teflon content to obtain variation in pore diameter and also hydrophobicity. On the top of the nano-porous layer, a thin layer of hydrophilic inorganic oxide (fumed silica) has also been deposited. They observed that the functionally graded nano-porous GDLs with hydrophilic layer showed an excellent fuel cell performance with a peak power density of about 0.46 W cm^{-2} at 85 °C using H_2 and air at 50% RH. The beneficial role of gradient in porosity in the removal rate of liquid water and in enhancement of the oxygen transport has also been highlighted by Chen et al. [30]. A carbon-filled GDL (CFGDL) proposed by Han et al. [31] showed a lower porosity of 67% and a smaller

average pore diameter of 4.7 μm and gave the largest limiting current density that reflected the improvement in mass transportation. Selvarani et al. [32] have reported the use of sucrose as the pore former in obtaining the porous structure in GDL and an enhanced fuel cell performance. Deyrail et al. [33] have reported a performance improvement for the GDLs by adding Montmorillonite nanoclay. Addition of 2 wt.% nanoclay lead to a porosity of 53% and a specific pore surface area of 75 $m^2 g^{-1}$.

2.3. Permeability

In a PEMFC, water in liquid-phase is produced during the operation. Water exchanges between the interface of the catalyst layer and micro-porous layer. It must be transported from the catalyst layer through the micro- and macro-porous layers of the GDL to the cathode flow-field. During the water transportation, the capillary pressure gradient must overcome the negative pressure gradient of the gas-phase. A low permeability and high flow resistance generate a high gas pressure gradient. The low permeability coefficients of GDL are associated with high liquid water saturation levels in the GDL. This is equivalent to a low effective porosity of GDL which ultimately affects the ability of oxygen to diffuse towards the catalyst layer. In integrated flow-fields, gas-phase is forced from high-pressure channels into the adjacent low-pressure channels through the GDL. In this case, the gas-phase is transported through the GDL mainly by convection with in-plane and through-plane velocity components, a few orders of magnitude higher than that in GDLs adjacent to conventional flow-fields. Permeability coefficients of the GDL components are important in understanding the relationship between chemical and structural properties of GDL and its functions for the cell.

The permeability coefficients define the types of the fluid transport as in-plane permeability (x, y directions) and through-plane permeability (z direction). The in-plane, through-plane, viscous and inertia permeability coefficients of macro-porous substrates and micro-porous layers have been determined separately by controlling the directions of the gas flow through the porous sample [34]. The permeability coefficients of the micro-porous layer are calculated from these two measurements. Since the viscous and the inertial permeability coefficients are independent of the fluid velocity, velocities much higher than that encountered during normal fuel cell operating conditions in GDLs adjacent to conventional flow-fields, but are within the range of velocities encountered in GDLs adjacent to integrated flow fields have been maintained in order to distinguish nonlinear effects. The permeability coefficients have been calculated using Darcy formula [34] and by application of the method of least squares to separate the quadratic term (inertial permeability) from the linear term (viscous permeability) on statistical basis.

Feser et al. [35] studied the permeability of samples of woven and carbon fiber-based GDL at various levels of compression using air as the impregnating fluid. Woven and non-woven samples have significantly higher in-plane permeability than carbon fiber paper at similar solid volume fractions. The following equation has been employed to calculate the in-plane permeability

$$\bar{\upsilon} = -\frac{k_i}{\mu}\frac{\mathrm{d}P}{\mathrm{d}r} \quad (2)$$

where $\bar{\upsilon}$ is the in-plane average fluid velocity, k_i is the in-plane permeability, μ is the fluid viscosity and $\mathrm{d}P/\mathrm{d}r$ is the radial pressure gradient.

Williams et al. [17] developed their own method of measuring the permeability of the gas flow through different GDL materials. With measured nitrogen flow rate and pressure drop across a substrate, the permeability coefficient representing gas permeability of the substrate was calculated using the following equation

$$k = \nu\mu\frac{\Delta X}{\Delta P} \quad (3)$$

where k is the permeability coefficient of the porous substrate, m^2; ν is the superficial velocity, calculated from the nitrogen flow rate divided by the area of samples, m s^{-1}; μ is the fluid viscosity = 1.8×10^{-5} Pa s for nitrogen at 23 °C; ΔX is the thickness of a substrate, m; and ΔP is the pressure drop across a substrate, Pa.

The extent of reactant bypass through the GDL from one channel to the others has shown the dependence on the GDL permeability [36]. On the basis of the radial flow technique, Feser et al. [35] determined the in-plane permeability of samples of woven, non-woven, and carbon fiber-based GDL at various levels of compression using air as the impregnating fluid. Woven and non-woven samples were reported to have significantly higher in-plane permeability compared to carbon fiber paper at similar solid volume fractions. Gostick et al. [37] studied the absolute gas permeability of several common GDL materials and reported that most materials displayed higher in-plane permeability than through-plane permeability. The permeability in two perpendicular in-plane directions showed the significant anisotropy with materials of highly aligned fibers showing the highest anisotropy. Shi et al. [38,39] employed the fractal permeability model for the GDL that accounted for the actual microstructures of the GDL in terms of two fractal dimensions, one relating the size of the capillary flow pathways to their population and the other describing the tortuosity of the capillary pathways. This model was found to be a function of the tortuosity fractal dimension, pore area fractal dimension, sizes of pore and the effective porosity of porous medium. Inoue et al. [40] reported that when the GDL effective porosity was small, the effect of gas flow through GDL became large and the current density distribution was not uniform. With the increasing of GDL permeability, the cell output density also will increase. He et al. [41] developed a fractal model to predict the permeability and liquid water relative permeability of the GDL and reported that water relative permeability in the hydrophobic surface is much higher than that in the hydrophilic case. Zou et al. [42] employed an unsteady model about single phase transport in cathode side of PEMFC with interdigitated flow field with both convection and diffusion processes. Two types of dynamic performances, start-up and state-to-state operations have been analyzed and it was found that the response time was generally quite fast, less than 0.1 s. The effects of GDL deformation on the flow cross-over due to the compression in a fuel cell assembly process has been investigated by Shi and Wang [43] using a three-dimensional structural mechanics model.

2.4. Transport properties

In a PEM fuel cell at high current densities, large amount of water is generated and condenses in the pores of electrodes and limited the reactant to access the active catalysts. This phenomenon of "flooding" is an important limiting factor of cell performance. It is important to minimize parasitic losses by proper management of reactants and water. Material optimization and design aspects are essential to achieve them by passive means which will enhance the net energy output of the cell. Many different approaches have been adopted so far to correlate the material properties to fuel cell performance qualitatively and quantitatively. Pasaogullari and Wang [44] studied the physics of water transport in both hydrophilic and hydrophobic diffusion media and concluded that liquid water transport across the GDL is controlled by capillary forces which are resulting from the gradient in phase saturation. Flooding diminished the cell performance as a result of decreased oxygen transport and surface coverage of active catalyst by liquid water. Using an optical H_2/air PEM fuel cell, Yang et al. [45] observed that water

droplets emerged from the GDL surface under oversaturation of water vapor in the gas-phase. It appeared only at preferential locations and grew to a size comparable to the channel dimension under the influence of surface adhesion. Energy, mass transfer and electrochemical kinetics in the gas distributor, GDL, catalytic layer and membrane have been mathematically modeled by Wohr et al. [46]. Rho et al. [47] have attributed the higher slope of the pseudo-linear region of the *I–V* characteristic curve with air or gas mixtures such as O_2/He, O_2/Ar, O_2/N_2 to mass-transport limitations in the active layer and the departure from linearity of the *E* vs. *I* plot to mass transport in the substrate-diffusion layer. They also inferred that by altering the Teflon content, porosity and/or thickness of this layer or by increasing the oxygen concentration in the gas mixture or increasing the pressure, mass-transport overpotentials in this layer could be considerably decreased. Neutron radio graphical measurements have been performed on operating PEM fuel cells to detect the liquid accumulation in flow field and GDL under various operating conditions [48]. Wang and Wang [49] estimated various time constants for important transient phenomena of electrochemical double-layer discharging, gas transport through the GDL and membrane hydration. They found out that the membrane hydration occurred over a period of 10 s, the gas transport of 0.01–0.1 s, with the double-layer discharging being negligibly fast. The results showed that the time for fuel cells to reach steady state was in the order of 10 s due to the effect of water accumulation in the membrane. A two-dimensional, two-phase, multi-component, transient model was developed and experimentally validated by Natarajan. Nguyen [50] showed the dominance of the dynamics of liquid water, especially in the high current density range on the cathode performance. With the help of fluorescence microscopy technique, Litster et al. [51] reported that the water transport is dominated by fingering and channeling rather than by the converging capillary tree. Studying by in situ neutron imaging, Zhang et al. [52] showed that material choice had considerable bearing on the presence of liquid inside the porous structures and the electrochemical characteristics. Wang and Wang [53] illustrated that the vapor-phase diffusion and capillary-driven liquid water transport in a GDL aid each other in water removal along the through-plane direction under the channel area, but oppose each other along the in-plane direction between the channel area and land. The backflow of liquid water was reported to increase with the increasing hydrophobicity and thickness, and decreasing pore size and porosity of the MPL [54]. Lin and Nguyen [55] studied the effects of the in-plane liquid water permeability and electronic conductivity of the GDL on cell performance and they inferred that more channels, smaller shoulder widths on the gas distributor, and higher in-plane water permeability of the GDL can enhance the transport of liquid water and oxygen, leading to better cell performance. Based on the three-dimensional numerical model developed to simulate the transport phenomena on the cathode side, Hwang et al. [56] predicted that the interdigitated gas distributor could give a higher average current density on the catalyst layer surface than that of parallel gas distributor under the same mass flow rate and cathode overpotential, while Cha et al. [57] found that for most flow pattern archetypes, optimal feature size occurred at an intermediate channel dimension. Using a two-dimensional model involving kinetics and mass transfer, Jeng et al. [58] predicted that the PEM fuel cell performance decreased with an increase in GDL thickness if porosity was low. Based on the analytical force balance model, Kumbur et al. [59] predicted the critical Reynolds number for water instability and suggested that for constant air velocity, droplet size and shape, reduced the channel height was preferred for effective water droplet removal. Aided by X-ray microtomography to obtain three-dimensional images of liquid water distribution in a GDL during gas purge, Sinha et al. [60] have reported that the drying rate decreased exponentially with the purge time and no significant liquid water removal taken place after 6 min of purge at room temperature.

Numerical simulation of the lateral transport of moisture and reactant was indicated by Wang and Wang [61] that a large pressure drop between two adjacent channels in counter flow caused severe reactant bypass between the two-flow paths of reverse directions which resulted in reactant flow short-circuit and lesser advantages of the counter-flow design. With the help of neutron radiography, the relative permeability and the liquid water saturation levels in GDL have been correlated [62]. A new method for estimating the internal contact angle to water and the surface energy of hydrophobic and hydrophilic gas diffusion media has been proposed by Gurau et al. [63]. Mennola et al. [64] indicated that at the cell temperature of 40 °C, the performance of the cell was limited by water removal whereas at 60 °C, the current distribution was determined by the partial pressure of oxygen.

Two-dimensional computational models to identify the mass transport limitations and evaluate the potential for passive regulation of temperature and oxygen supply [65] and gas transport enhancement using baffle plates [66] have been reported. The adhesion force between the liquid droplet and the solid surface and its change for the removal of the water droplets has been studied [67]. The importance of the anisotropic microstructure of the fibrous electrodes to model the effective transport coefficients has been highlighted by Pharoah et al. [68]. Water transport in air-breathing PEMFCs is interpreted in terms of the net water drag coefficient [69]. The dynamics of GDL dewetting has been analyzed [70] and reported that the water diffusivity in the anode GDL was several times larger than that in the cathode leading to faster water loss of the anode side to the dry gas stream. The importance of increased porosity of the GDL to achieve a higher cell performance in the case of interdigitated flow field mass transfer by forced convection has been highlighted [71]. The ionic conduction influencing the cathode performance over a wide range of current densities and the gas-phase transport affecting the cathode performance at high current densities have been brought to light by Guo et al. [72]. By designing fuel cells with enhanced in-plane convection by the way of increasing in-plane permeability of the GDL and channel length, the losses associated with low oxygen content and liquid water buildup in the catalyst layer have been reported to be reduced [73]. The ranges of water vapor condensation and liquid water evaporation were identified across the thickness of the GDL by Song et al. [74] who reported that evaporation occurred within GDL close to the channel side and condensation close to the catalyst layer side. Impedance technique was employed by Bultel et al. [75] to evaluate the oxygen depletion due to the slow diffusion in GDL when using air at the cathode.

Pore-network model proposed by Sinha and Wang [76] revealed finger-like liquid waterfronts and liquid coverage at the GDL–channel interface, resulting in pressure buildup inside the GDL and breaking out of liquid water from preferential locations. The permeability coefficients of GDL with varying PTFE content and carbon types were calculated [34] using Darcy-Forchheimer and reported that higher PTFE content resulted in high in-plane and through-plane viscous permeability coefficients which also depended on the carbon type. Studies of pressure distribution and flow cross-over through the GDL using Darcy model [77] revealed that an increase in Reynolds Number could lead to the increment in the flow cross-over, whereas using the conservation laws governed the multi-phase flow. On each side of the moving boundaries, the nonlinear system has been approximated by its linearization whose relaxation times were reported to be shorter than the front evolution [78]. Wet-proofing of GDL with tetrafluoroethylene–hexafluoropropylene was reported to be effective for the application that required the operation at relatively high potential and high utilization of air [79]. The modeling results by

Liu and Zhou [80] showed that the PEM fuel cell with interdigitated flow field would outperform that with conventional flow field due to mass transfer enhancement of forced convection through the GDL. A new detector technology, based on micro-channel plates has been proposed by Hussey et al. [81] for the direct measurement of the through-plane water distribution in the GDL. A study on cross flow through GDL as a function of flow rate, permeability and thickness of GDL highlighted the effects of those parameters on the resultant cross flow and the pressure drop of the reactant streams [82]. Fairweather et al. [83] developed micro-fluidic device for measuring the capillary pressure as a function of liquid water saturation for these thin porous materials in order to understand and optimize the liquid water transport in GDL. A two-fluid model by He et al. [84] showed that a high contact angle and a low surface tension were advantageous for liquid water removal in the gas channel and the GDL even though a low surface tension would lead to a low capillary force in the GDL.

Flooding of the GDL hydrophobic pores with diameter greater than the capillary condensation threshold diameter and the role of the unflooded pores as passageway for gas transportation and the availability of the corresponding catalyst area for electrochemical reaction were studied by Liu et al. [85]. The effects of the flow channel area ratio on the reactant gas transport, the cell performance of PEMFCs with parallel and interdigitated flow channel designs were analyzed to show that the flow channel area ratio and liquid water distribution significantly influenced cell performance at lower voltages [86]. The changes of relative permeability and capillary pressure as a function of liquid water phase saturation have been investigated by Markicevic et al. [87] using a capillary network model and shown that relative permeability was constant for low saturation, but followed a power law of saturation for high saturations, with an exponent of about 2.4 which was independent of network size or heterogeneity. Numerical solution of the equations concerning the isothermal multi-phase multi-component flow in the GDL has been deduced by Vynnycky [88]. The model by Weber and Darling [89] clarified the role of the porous plates in humidifying dry reactant streams and managing liquid water. The simulation of the liquid–gas two-phase transport using the multi-phase mixture model as applied to a carbon-fiber paper GDL has been reported [90].

An isotropic numerical treatment of the anisotropic electron transport phenomenon in PEM fuel cells has been proposed [91]. The hydrophilicity of graphite plate and the hydrophobicity of GDL have been shown to play an important role in the liquid water motion [92]. Chang et al. [93] reported that the liquid water generated by the electrochemical reaction could significantly reduce the effective porosity of the GDL under high current density conditions, thereby hindering oxygen transport through the GDL. The computational model developed by Gurau et al. [94] for the study of the dynamics of water transport, the impact of the GDL and catalyst layer properties on the amount of water retained in the fuel cell components revealed that the GDL permeability and its pore size at the interface with the channel determine the amount of water retained in GDL while that in the cathode catalyst layer is determined by the saturation equilibrium at the interface with the GDL. Better water transport in carbon-cloth GDL over carbon-paper GDL under humidified conditions was attributed to broader pore distribution of a carbon-cloth GDL, thus creating oxygen-diffusion paths even if water accumulated [95]. The capillary pressure and relative permeability of the carbon-fiber paper GDL have been correlated to identify the two-phase multi-component transport in the GDL. The wetting behavior of the GDLs and the conditions leading to the onset of pore plugging [96] has been modeled. The possibility of phase change of water in GDL incorporating the effect of hygro and thermal stresses has been modeled [97]. The temperature difference between the solid matrices and the fluids in the diffusion layers decreasing with increasing the non-dimensional interfacial heat transfer coefficient has been proposed by Hwang et al. [98]. A two-dimensional theoretical model by Tsai et al. [99] proposed that the concentration flux of oxygen across the GDL was primarily dominated by the thickness and porosity of GDL. For a thicker GDL, the diffusion resistance increased while the increase of porosity enhanced the transport of oxygen and cell performance.

A numerical investigation by Chiang and Chu [100] with various channel aspect ratios and thickness of GDL revealed that a slender channel was suitable for cells operating at moderate reaction rate, and a flat channel could produce more current at low cell voltage. A two-dimensional numerical model by Jang et al. [101] based on the porosity and thickness of the GDL showed that increasing the porosity of GDL causes the increasing of mass transfer of the reactants and results in higher performance.

As significant convective transport occurs in porous media for practical fuel cell conditions, the use of flow field design from a hydrodynamic perspective has been suggested to minimize the effects of the parasitic loads [102]. Based on the numerical model Hu et al. [103] have reported that dead-ended structure of an interdigitated flow could increase the oxygen mass fraction and decrease the liquid water saturation in the GDL as compared to the conventional mode of flow. The slow transient effects of liquid water accumulation and evaporation in the GDLs and gas channels have been modeled by Promislow et al. [104]. The advantages of hydrophobic GDLs in terms of the pore scales have been simulated by pore-network model [105]. The GDL modified by laser-perforation with respect to the flow field design has been reported to have better dynamic and overall performance of the fuel cell [106]. Potential-step voltammetry and nonlinear low-frequency impedance have been proposed as quick alternatives to neutron radiography for the study of the two-phase flow in the GDL to provide information on the change of the liquid saturation with time [107]. Using high-resolution neutron radiography, Hickner et al. [108] examined the cross-sectional liquid water profile and have reported that at 60 °C, the water content in the center of the GDL was depleted compared to the membrane or gas flow channel interfaces. Sinha and Wang [109] reported that in a PTFE treated, mixed wet GDL, liquid water preferentially flew through connected GDL hydrophilic network suppressing the finger-like morphology observed in a wholly hydrophobic GDL. A dynamic interconnection of water pathways within the GDL has been proposed by Bazylak et al. [110] based on a fluorescence microscopic study and supported by computational fluid dynamics (CFD) simulations. Though an interest in interdigitated flow channels is gaining momentum, Lee et al. [111] have shown that there is also an increase in friction due to the strong convection through the porous diffusion layer accompanied by a larger pressure drop along the flow channel. By the visualization technique, it has been shown that water blockage to the air flow path was caused by the overlapping of two land-touching droplets developing on each side of the channel. Flooding was reported to be more susceptible to the air flow than the other test operating conditions [112]. Park et al. [113] showed that the permeability of porous medium was strongly dependant on the fiber tow orientation in three-dimensional simulations by the efficient numerical scheme of the lattice Boltzmann method. The same method has also been reported by Niu et al. [114] to simulate the water-gas flow in the GDL and investigate the saturation-dependent transport properties under different conditions. The wetting behavior of the GDLs and conditions leading to the onset of pore plugging have been reported using 3D, multi-phase and nonisothermal model [115]. The water transport phenomena and the transient behavior in the GDL have been theoretically studied by Yan et al. [116]. The numerical optimization of the thickness and porosity of GDLs have been carried out by Grigoriev et al. [117]. A method and apparatus for measuring the relationship between air–water capillary pressure

and water saturation in PEMFC GDLs have been described and a permanent hysteresis between water intrusion and water withdrawal have been demonstrated [118]. An accelerated numerical investigation of air-water flow across a GDL using computational fluid dynamics software has been reported [119]. Radial biasing has the beneficial effects of decreasing the network saturation and a desirable quality in GDLs. It was reported that small radial biasing could yield a 43% decrease in average saturation compared to pore networks without a prescribed radial gradient [120]. Using the capillary pressure to determine the slip velocity between the phases, the Maxwell–Stefan equation was used to model the diffusive fluxes of the multi-component gas mixture in the GDL [121]. The capillary properties of the GDL have been shown to have a more significant effect on the fuel cell performance and better fuel cell performance was obtained with GDL and catalyst layer with high capillary diffusion capability and low hydrophilic porosity [122]. The water and thermal management in PEMFCs were reported to depend on the permeability characteristics of the GDL [123]. A literature overview of computational models, ranging from one-dimensional, single-component to complete three-dimensional has been presented with emphasis on heat and mass transfer [124]. With the aid of neutron radiography the performance of a polymer electrolyte membrane (PEM) fuel cell based on, the effects of liquid water accumulation in the GDL have been projected [125]. Adopting an agglomerate catalyst layer (CL) model, the transport processes within the GDL, the CL and the transport/reaction processes within an individual agglomerate particle have been elaborated by Jain et al. [126].

GDLs with the dry micro-porous layers were reported to exhibit better electronic conductivity and more stable hydrophobicity than those with the wet layer MPLs [127]. Using synchrotron X-ray imaging technique, the mechanism of water flow within the fuel cell and the relationship between water behavior and cell performance have been reported [128]. The wettability of the micro-channel surface has been shown to have a major impact on the dynamics of the water droplet, with a droplet splitting readily and converting rapidly on a hydrophobic surface, while for a hydrophilic surface there is a tendency for spreading and the film flow formation [129]. It was reported that the water droplet tended to become unstable when decreased the channel height or increased the flow velocity or making the GDL dried [130]. The time evolution of the advancing and receding contact angles of the droplet have been found to be sensitive to the wettability when the GDL surface is hydrophilic, but it was independent of wettability when the surface is hydrophobic. The critical air velocity at which a droplet detaches was found to decrease with the increasing of hydrophobicity and the initial dimension of the droplet [131]. Using the artificial neural network simulations, Kumbur et al. [132] have proposed that tailoring the DM with high PTFE loading and applying high compression pressure could lead to a higher capillary pressure thereby promoting the liquid water transport within the pores of the DM. Any increment in hydrophobicity of the DM was found to amplify the compression effect which would yield a higher capillary pressure for the same saturation level and compression. By particle image velocimetry, velocity maps of primary and secondary flow within the channels were obtained [133] and reported that significant portions of the flow travel between adjacent channels occurred through the porous medium. With the help of the micron- and millimeter-scale sensors, Fabian et al. [134] have shown that thermal and species concentration effects were not confined to the GDL, but extended well beyond the cathode surface. Transient data also revealed substantial differences in the time constants associated with oxygen, water and heat transport. Mathematical model for flow of a multi-component mixture of ideal gases in a highly porous electrode [135] has also been reported. The effect of vapor-exchange processes in the GDL on the overall cathode performance has been studied [136].

Studied the dynamic behavior of a five cells stack operating in dead-end mode, Mocoteguy et al. [137] have indicated that water management issue in a fuel cell operating in dead-end mode at room temperature mainly consisted in avoiding pore flooding instead of providing enough water to maintain membrane conductivity. To minimize the problem of water flooding, provision of a slit and groove in the cathode GDL has been proposed by Nishida et al. [138,139]. A discussion on the pore-scale models coupled with realistic microstructural delineation, as well as micron-resolution imaging techniques for studying the influence of the underlying structure and surface wettability on liquid water transport and interfacial dynamics in the fuel cell GDL, has been reported [140].

Lot of research articles have appeared on another important aspect of PEMFC, the water management. Several experimental, numerical, computational studies have been carried out in addition to 1D, 2D and 3D modeling of the GDL to explore the characteristics and conditions influencing on the fuel cell performance. Table 1 summarizes the details of the characteristics studied in several publications and the inferences deduced [141–215].

2.5. Electron transport

The lateral electronic resistance of GDL is affected by the electronic conductivity, GDL thickness, and gas channel width [216] which plays a critical role in determining the current distribution and cell performance. There is an increasing interest in analyzing the current distribution and the data obtained [217] show the effects of cathode stoichiometry variation and transient flooding on local current density. A measurement system for the mapping of current distribution in a free-breathing PEMFC has been proposed and reported that the current density profile was more homogeneous at elevated temperatures [218]. A three-dimensional numerical model suggested by Lee et al. [219] indicates that insufficient water would lower the conductivity of the membrane and yield low currents at a fixed voltage. The electrical contact resistance between GDLs and bipolar flow channel plates is one of the crucial factors contributing to the operational voltage loss in PEMFC. A fractal asperity based model has been adopted to predict the contact resistance as the functions of pressure, material properties, and surface geometry [220]. The current distribution measurement system by Noponen et al. [221] distinguishes between current distribution originating from differences in proton conductivity, species concentration and GDL properties. For current distribution studies, Natarajan and Nguyen [222] have recommended segmenting the electrode along with the current collector. The contact resistance between the bipolar plate and the GDL has been analyzed by contact resistance-pressure constitutive relation [223]. A numerical investigation of the coupled electrical conduction and mass diffusion in the cathodic GDL of a PEMFC has been carried out using 2D simulations [224]. The results showed that the current density distribution under the land area could be dominated by either electron transport or mass transport, depending on the operating regime. The analysis of the in-plane current density gradients showed the contributions due to electrical conduction, oxygen diffusion and membrane resistance. A simple technique was developed to measure current distribution in PEMFC with serpentine flow fields [225]. Considering the electron conductors in a plane perpendicular to the channel direction as two-dimensional resistors, Freunberger et al. [226] showed that electrical and ionic resistances seemed to govern the current distribution at low current regimes, whereas mass transport limitations locally hampered the current production at high loads. The contact resistance between the bipolar plate (BPP) and the GDL in a PEMFC constituted a significant portion of the overall fuel cell electrical resistance and a micro-scale numerical model was developed to predict the electrical contact resistance between BPP and GDL by simulating the

Table 1
List of research articles emphasizing on the water management aspect in PEM fuel cell.

S.No.	Characteristics studied	Inferences made	References
1.	Neutron imaging: in situ non-destructive analysis	Water in the cell flow channels and in the GDL imaged	[141]
2.	Two modes of liquid water removal from the GDL surface	Shear force and capillary wicking	[142]
3.	Numerical model for two-phase flow and transport of species	Humidification level and flow rate determine performance	[143,144]
4.	Effect of water flooding in the GDL	More severe in catalyst layer than in GDL	[145]
5.	GDL with water management layer	Resulted in improved water management	[146]
6.	PEMFC under dry operation	Net power output drop by 17% but energy need cut by 46%	[147]
7.	Water flow through carbon cloth and carbon paper GDL	Small pores remain free of water and permit gas	[148]
8.	Water transport in GDL	At high water transport the ionic resistance lower	[149]
9.	Freeze degradation study	GDL got changed by the first freeze cycles	[150]
10.	Water phase during startup from sub-zero temperatures	Freezing-point depression of water plays negligible role	[151]
11.	Cold start	Additional flow sharing problems occur in fuel cell stack	[152]
12.	Onset of instability leading to water removal	Enhanced by increasing flow channel length, gas flow velocity, decreasing channel height and making the GDL interface more hydrophobic	[153]
13.	Water absorption layer between gas and waste channels	Gas flowing in the layer is not blocked	[154]
14.	Cold-start behavior and the effect of sub-zero temperatures	Catalyst layer delamination from membrane and GDL leading to hydrogen cross-over	[155]
15.	Transport and electrochemical processes at sub-zero start up	Accounts for ice/frost precipitation and growth in GDL	[156]
16.	3D visualization of the water distribution in the gas diffusion medium	Only a small number of pores are occupied by liquid water at breakthrough	[157]
17.	Effects of varying ambient temperature and relative humidity	Membrane changed from fully hydrated to dried out state at a GDL temperature of approximately 60 °C	[158]
18.	Integrated planar electroosmotic pumping structures	Improves fuel cell performance and stability	[159]
19.	1-dimensional model of the GDL	Cell performance as a function of GDL properties	[160]
20.	Water removal capacity of the GDL materials	No liquid water in the anode flow field unless cathode GDLs had a micro-porous layer.	[161]
21.	Structure–performance relationship for GDL	Performance differences between carbon paper and carbon cloth	[162]
22.	Stack shut-down protocol in subfreezing weather	Self-start is faster if the metal bipolar plates are used	[163]
23.	Auto-humidified operation of channel-less, self-draining fuel cell	Operates well on dry feeds	[164]
24.	Gas-phase transport in GDL and the catalyst layer	Overpotential distributions determined	[165]
25.	GDL wettability on water distribution in the anode	Slight increase in anode plate temperature avoids surface condensation and anode flooding	[166]
26.	Water management system with external electro-osmotic pump	Facilitates high volumetric power density at all operating conditions	[167]
27.	Three GDLs with different micro-flow channels	Designs of GDLs affect the liquid water flow patterns	[168]
28.	Capillary-induced flow in thin-film GDL with mixed wettability	Effect of permeability and wettability on saturation profiles	[169]
29.	Dynamic behavior of liquid water in GDL pores	Critical air inlet velocities for droplet detachment calculated	[170]
30.	Effects of freezing conditions on GDL properties	GDL more resilient to material loss in the absence of water phase transitions	[171]
31.	Location of the gas–liquid interface in GDL under various RH	Liquid interface approaches the gas flow channel inlet and liquid water obstructs the pores in the porous media	[172]
32.	Cell performance and the flooding behavior	Depended on wetting properties of GDLs	[173]
33.	Review on water management	Two classes of strategies to mitigate flooding proposed	[174]
34.	Simultaneous heat and mass transfer in the cathode GDL	Latent heat effects due to condensation/evaporation of water strongly affect the two-phase transport	[175]
35.	High-temperature PEM fuel-cell stack (120 °C)	Optimization of membrane, cathode catalyst layer, GDL	[176]
36.	Dynamic behavior of fuel cell stacks	Liquid water accumulates in the cathode in the GDL until a critical saturation fraction is reached	[177]
37.	GDL flooding	Effect of homogenous GDL flooding analyzed	[178]
38.	Water management in the air flow channel by volume of fraction (VOF) model	Hydrophilicity of reactant flow channel is critical for water management	[179]
39.	Effects of residual water in PEM fuel cell after cold start	Change of mass-transport process originated from GDL	[180]
40.	Reaction and thermal flow analysis	Optimal flow pattern of gas and cooling water could make the relative humidity higher and more uniform	[181]
41.	Thin cast Nafion membranes for non-humidified conditions and at various temperatures	Better back-diffusion of water and lower membrane resistance, high efficiency with low-porous GDL	[182]
42.	Water freezing phenomena	Ice formation between GDL/MEA interface causes air gas stoppage	[183]
43.	Gas purge for successful start-up	Low RH of purge gas, high gas flow rate, and high cell temperature favor effective purge	[184]
44.	Dynamic performance during startup or load change processes	Determined by the cathode flooding and oxygen transport in the GDL	[185]
45.	Local current density distribution at the membrane–GDL interface	Cathode water accumulates in shoulder area and congests the pores of the GDL affecting current density	[186]
46.	Performance of a self-humidifying PEMFC and amount and distribution of water as observed using H-1 NMR	Decline of the power density occurs by the accumulation of H_2O (l) in the GDL and cathode flow field	[187]

Table 1 (*Continued*)

S.No.	Characteristics studied	Inferences made	References
47.	Dynamics of stirred tank reactor PEMFC	Effects of temperature, external load resistance, inlet hydrogen and oxygen flow rates on current evolution	[188]
48.	Water management layer (WML) onto a traditional GDL	Balance of water with WML in the fuel cell	[189]
49.	Fuel cell stack characterization and electrochemical response	A semi-empirical electrochemical model of GDL porosity and electro-osmosis coefficient of membrane proposed	[190]
50.	Effect of GDL on the cell water management	Characteristics of GDL influence membrane hydration and inlet humidity on anode side has major effect on flooding at the cathode	[191]
51.	Simulation of polarization curves and ohmic overpotential	Effects of liquid water in both the GDL and catalyst layer, cathodic transfer coefficient need to be focused	[192]
52.	Repulsive Kelvin forces acting on liquid water through a porous the GDL by magnet particles	Mechanism of the improvement of the cell performance by magnet particles is clarified	[193]
53.	A coupled electron and two-phase mass transport model for anisotropic GDLs	GDL with deformation shows high concentration polarization	[194]
54.	Water distribution in a PEMFC by X-ray imaging technique	Water distribution in region between separator and GDL evaluated	[195]
55.	Interaction of water droplet with solid wall on hydrophobic GDL	Hydrophobic land areas are preferable for mitigating the accumulation of liquid water in the gas flow channels	[196]
56.	Single cell as a lumped model with 15 interconnected segments	Current density, water content in the membrane, RH in the flow channels and water accumulation in GDL predicted	[197]
57.	Water transport rate across the GDL	Water rejection rates across a GDL at different cathode air flow rates measured	[198]
58.	Synchrotron radiography and tomography study of water droplets in GDL	Water cluster in the range of several nano-liters detected	[199]
59.	Multi-phase multi-dimensional model for cold-start simulations	Low interfacial water vapor concentration at GDL and gas channel surface on cathode side delay ice formation	[200]
60.	Flooding analysis of a single PEMFC by impedance study	The onset of flooding sensitive to the design of GDL	[201]
61.	Accumulation of liquid water within the PEMFC	Rate of accumulation of liquid water, its impact on the rate of cell voltage drop deduced	[202]
62.	Dynamic water transport in the porous layers of PEMFC	Capillary pressure, relative permeability and oxygen diffusivity determined	[203]
63.	Computational fluid dynamics analysis of GDL permeability	Water management was good in systems in which the permeability in at least one direction (in-plane or through-plane) was high	[204]
64.	Performance testing of commercial diffusion media	Existence of a strong and complex interaction between the macro- and micro-porous layers of the gas diffusion electrode	[205]
65.	Transport of liquid water in the cathode GDL	Liquid water saturation increases with temperature	[206]
66.	Review on water management in GDL	Microscopic flow of liquid water through the membrane, catalyst layers and GDL	[207]
67.	Effects of the flooding of GDL	GDL porosity, thickness and mass transfer at the GDL-gas channel interface reported	[208]
68.	Microstructured flow field for passive water management	New flow field design stabilized the cell performance	[209]
69.	CFD analysis of the reactants flow and water management	Depended on anode humidification and the related water management	[210]
70.	Lattice Boltzmann model for the multi-phase flow phenomenon in the inhomogeneous GDL	Simulates the unsteady behavior of liquid droplet motion in the porous medium	[211]
71.	Relationship between a flooding and PEMFC voltage drop	Cell voltage decreased with time and was accelerated by larger current and smaller air flow rate	[212]
72.	Ratio of liquid water to pore volume in GDL	Water saturation changed with cell operation conditions	[213]
73.	Mass transfer in porous gas diffusion medium	Fraction of water-flooded pores calculated as a function of structural parameters of the porous system	[214]
74.	Water flow dynamics	Water management that balances membrane dehydration with electrode flooding deduced	[215]

BPP surface topology and GDL structure under the normal operation conditions [227]. The contact resistances between the GDL and CL have been shown to decrease nonlinearly as the GDL thickness decreased due to the compression pressure [228]. Total through-plane electric resistance of the GDL and the catalyst layer under different compressions have been measured [229] and the results showed that the difference between the total through-plane electrical resistance under the channel and the shoulder was large enough to cause the higher current density under the shoulder. Chirkov and Rostokin [230] performed an analysis of the way to make the GDL restrict the process of generation of current in a cathode and of what measures should be taken in order for the extraneous diffusion restrictions to become less significant. The equivalent electric-circuit for PEMFC to obtain numerical distributions of hydrogen/oxygen concentrations, cell potential, current density, and gas/cell-component temperatures has been reported by Onda et al. [231]. Using a theoretical contact mechanics model, Barber et al. [232] reported that smoother materials, thicker gold coating, and higher clamping force resulted in a higher real percentage contact area. Nonzero contact stress was required to maintain low electric resistivity in the PEMFC. Stress relaxation in the membrane–electrode assemblies has been studied [233] by modeling the membrane as a porous-viscoelastic solid, and the GDL as a nonlinear elastic solid. A two-dimensional two-phase model was used to analyze the effects of anisotropic electrical resistivity on current density and temperature distribution by Bapat and Thynell [234]. It revealed that a higher in-plane electrical resistivity of the GDL adversely affected the current density in the region adjacent to the gas channel. Current distribution to highlight the membrane resistance [235], the contact resistance between the bipolar plate and GDL as predicted by finite element methods [236,237] and non-isothermal, two-phase model [238] underscore the importance of optimization of cell geometry. The study of the internal properties, such as gas velocity distribution, mass fraction of the reactants, fraction of water, and current density distribution in the electrode and GDL revealed that the co-flow mode improved the current density distribution with humidified normal condition compared to the counter-flow mode [239].

The micro-porous layer (MPL) consisting of carbon black powder and hydrophobic agent is utilized on one side or two sides of the GDL. This layer is the crucial part in GDL to improve the fuel cell performance as it acts both as a valve that pushes water away from the GDL to the flow field to minimize water flooding and also transports the input gas from flow field into catalyst layer. So it is one of the bottlenecks in fuel cell developments, and many R&D activities during last decade have accomplished amazing achievements in this area. Williams et al. [17] estimated various physical parameters of the GDLs coated with the MPL such as in-plane electronic resistivity, hydrophobicity, gas permeability and pore size distribution. The effects of Teflon and carbon loadings in MPL have been studied [240–243]. Wang et al. [20] have used composite carbon black consisting of Acetylene Black and Black Pearls 2000 carbon on a novel MPL. Kannan et al. [244,245] have reported that using Pureblack carbon as the material for the fabrication of micro-porous layer performed better than Vulcan-XC72R.

2.6. Compression

The amount of compression on the GDL affects the contact resistance, the GDL porosity, and the fraction of the pores occupied by liquid water and ultimately the performance of PEMFC. Over-compression commonly exists in the fuel cells. To explore the effects of GDL compression on fuel cell performance, several studies have been carried out to highlight the decrease in fuel cell performance with increase in compression [246], degradation of the GDL under compression leading to the formation of preferential pathways for water transport. Scanning electron microscopy used to investigate the effects of compression on the morphology of the GDL and it showed that compressing the GDL causes the breakup of fibers and deterioration of the hydrophobic coating [247]. It has been observed that decreasing the stress applied on the GDL would increase durability of the MEAs and have a positive effect on their performance [248]. The GDL is compressed very little under the channel whereas under the rib it is compressed to gasket thickness. The compression of GDL reduces gas permeability and contact resistance, and improves bulk conductivity. Nitta et al. [249] reported that the inhomogeneous compression of GDL might lead to significant local variation of mass and charge transport properties in the GDL.

Using the Finite element method and finite volume method, Zhou et al. [250] studied the elastic deformation of the GDL, the mass transport of the reactants and products and reported that there existed an optimal clamping force to obtain the highest power density for the PEMFC with the interdigitated gas distributors. The effect of clamping force on the interfacial contact resistance and the porosity of the GDL has been studied. It has been inferred that there existed an optimal rib width of the bipolar plates to obtain a reasonable combination of low interfacial contact resistance and good porosity for the GDL [251]. In the case of fuel cell stacks, too much pressure might result in damage to the GDL and uneven distribution of the contact pressure which would result in hot spots. Using finite element analysis procedures for the fuel cell stacking assembly were established by Lee et al. [252] to determine the proper stacking parameters such as stacking design, bipolar plate thickness, sealing size and assembly pressure. Using the GDL parameters as the input, the model developed by Hottinen et al. [253] indicated that inhomogeneous compression can have significant effects on the lifetime and local performance of the cell. The numerical method by Zhou and Wu [254] outlined the effects of the compression deformation on the contact resistance, GDL porosity distribution and the cross-section area of the gas channel. The effects of the clamping pressure on porosity, gas permeability, electrical resistance and GDL thickness have been determined by Chang et al. [255].

The effect of inhomogeneous compression of GDL on the temperature distribution [256], transport properties [257], the gas permeability, bulk density, thickness and conductivity of two types of GDL [258], the mechanical and thermal properties of GDL [259], extrinsic properties such as porosity and permeability [260] and the performance of PEMFC with respect to ohmic and mass transport polarizations [261] have been studied. Fekrazad and Bergman [262] reported that the fuel cell stack performance in terms of power output and internal temperature distributions is very sensitive to the compressive load. Using a reduced model for the compression of the GDL, the influence of the compression on permeability, diffusivity and heat conductivity as the function of the saturation of the porous medium has been studied [263].

2.7. Structure

Structure plays an important role in defining the functionality of the GDL. The cross-sectional view of GDLs reported in literature reveals a gradient in the pore size from the macro-layer to the micro-layer. To bring about the structural modifications to the GDL and impart the required balance of hydrophilicity and hydrophobicity, several treatments have been reported. The GDL layers are typically containing the macro-porous gas diffusion backing and micro-porous layer. The micro-porous layer consisting of carbon black powder and hydrophobic agent is utilized on one side or two sides of the GDL. This layer is the crucial part in GDL to improve the fuel cell performance as it acts both as a valve that pushes water away from the GDL to the flow field to minimize water flooding and also transports the input gas from flow field into catalyst layer. So it is one of the bottlenecks in fuel cell developments. But many R&D

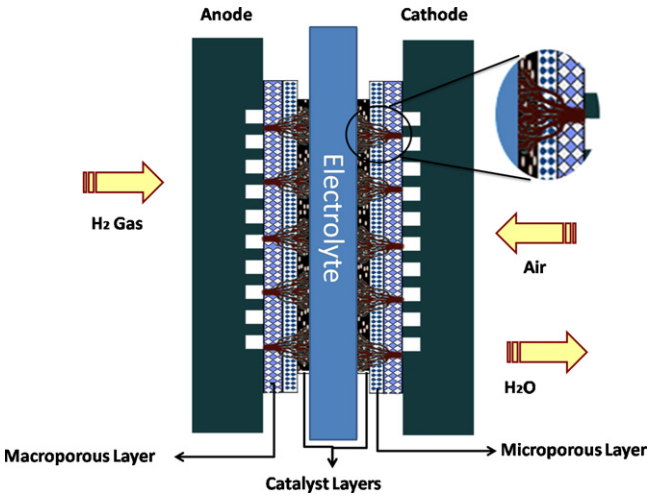

Fig. 4. Membrane–electrode assembly configuration showing the capillary force to absorb the input gas and output water in the GDL.

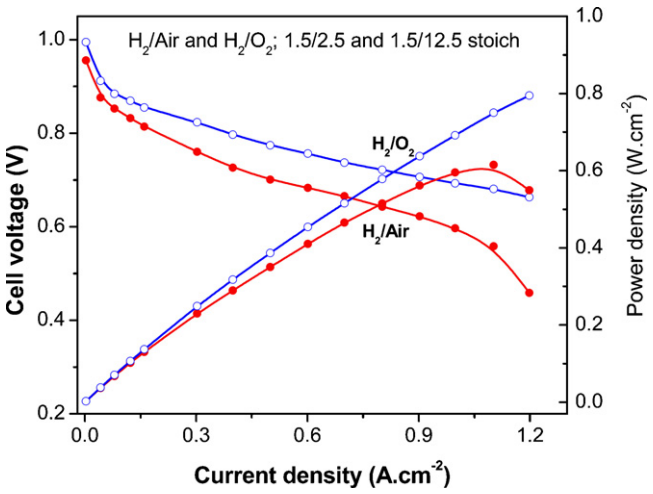

Fig. 5. Fuel cell performance of Nafion-212 based MEA at 80 °C using H_2/air and H_2/O_2 (100% RH) at 1 atmosphere back pressure.

activities during last decade have accomplished amazing achievements in this area. The functions of the micro-porous layers are to facilitate effective distribution of the reacting gas to the membrane surface and provide mechanical compatibility between the layers with minimum contact resistance and assist in water management.

Fig. 4 shows the micro-porous channels in the micro-porous layer which have the strong capillary force to absorb the input gas and output water. Under the assumption that all the pores are cylindrical, the capillary law illustrates the relationship between pore diameter d_p and the applied pressure p,

$$d_p = \frac{4\gamma \cos\theta}{p} \quad (4)$$

where γ and θ denote the surface tension and the contact angle with the micro-porous layer, respectively.

The macro-porous layer of the GDL is either carbon paper or woven carbon cloth and it serves as a current collector, a physical substrate for the catalyst layer and an elastic component of the MEA. The macro-porous substrate provides mechanical support as well as connection between the flow field and micro-porous layer. In general, overall impedance of the cell comprises the bulk resistance as well as contact resistance between electrodes and electrolytes in addition to GDL/bipolar plates. The contact resistance could be higher between the bipolar plates and the GDLs due to the flow channels (see MEA configuration in Fig. 4) compared to that between GDLs and Catalysts layers. Hence, the MEA configuration and structure are very critical for achieving lower overall impedance and higher power density.

Chen-Yang et al. [264] reported a series of PTFE/carbon black composite-based single-layer GDL and the PTFE resins being homogeneously dispersed in the carbon black matrix and exhibited a micro-porous layer like structure. POLYMET a polymer with a three-dimensional polymeric structure metallized with the enclosing, coating of different kinds of metals or alloys has been proposed [265] as GDL material due to the wide ranges of tailor-made, micro-porous structures on a designable scale. Nanostructured components are introduced in MEA to improve the functionality by the structural refinement. Kannan et al. [266] have reported the single-walled and multi-walled carbon nanotubes supported platinum to fabricate the GDL and the catalyst layers in the MEAs, respectively with excellent GDL surface morphology. Using these nanostructured components, the fuel cell tests exhibit the promising performances either using the hydrogen–air or hydrogen–oxygen as the reactants at ambient pressure. A mathematical model to describe the microstructure of the GDL of PEMFC, based on tools from stochastic geometry has been attempted by Thiedmann et al. [267]. The GDL has been considered as a stack of thin sections based on the visual appearance of relevant microscopic images. The thin sections have been modeled as planar (2D) random line tessellations which have been dilated with respect to three dimensions.

3. Fuel cell performance

As seen from Fig. 5 the fuel cell performance (peak power density) with H_2 and O_2 as reactants is very high compared to that with H_2 and air. Even the open circuit voltage is ~15 mV higher for the case with O_2 as oxidant due to a portion of the Nernst equation $RT/2F$ ln(1/0.21). With proper design of the GDLs, the reduction in power density when using air as an oxidant can be minimized. For example, the power density observed using air is about ~0.6 W cm^{-2}, even though the partial pressure of oxygen is only 0.21 in air. The relatively high performance with H_2 and air is due to the optimum properties of hydrophilic/hydrophobic balance, conducting network, pore dimension, distribution, etc. In the literature, several strategies have been explored in order to have high performance when using H_2 and air.

One of the approaches was to use various types of carbon powders like oil-furnace carbon black, acetylene-black, partially graphitized Pureblack carbon, aligned carbon nanofibers, aligned carbon nanofibers/Vulcan carbon composite, graphitized polyacrylonitrile carbon, carbon nanotube free-standing membrane, metallic porous medium (copper foil), carbon fiber reinforcing materials impregnated with different phenolic resin, pore forming agents, pitch-based carbon materials (mesophase pitch and coal tar pitch), vapor grown carbon nanofiber (VGCF) in the carbon black/poly(tetra fluoroethylene) composite, PAN-based carbon fiber cloth, Carbon fiber paper with 10 wt.% phenolic resin and carbon fiber paper with phenolic resin, carbon black [244,268–283].

There are also several publications dealing with GDL designs, like porous gas diffusion half-layers, secondary pores [284–286]. There are several studies using two-dimensional, pseudo 2D modeling of oxygen diffusion, three-dimensional, isothermal and multiphase numerical modeling with a focus to optimize the transport phenomenon of the GDLs to improve the fuel cell performance [287–297]. In order to understand and optimize the fuel cell performance at a wide operating RH range, various properties of GDLs

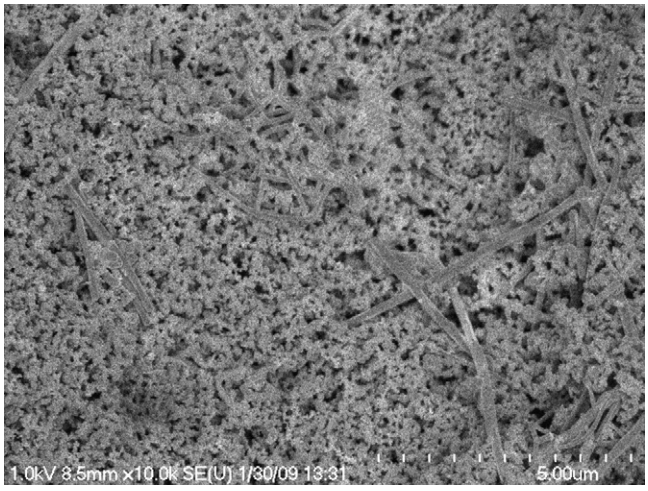

Fig. 6. Scanning electron micrograph of a micro-porous layer fabricated by wire rod coating process.

such as porosity, high frequency resistance, surface morphology, Gurley porosity, etc. have already been studied [298–301].

4. Coating processes

The preparation of the GDL has been reported by rolling, spraying, and screen printing methods and the impregnation of the Nafion solution by spraying and brushing methods. With the carbon paper or the carbon cloth as the support structure (macro-porous layer), the preparation of the GDL is widely based on spray technique. Kannan et al. [302] have proposed the use of the wire rod coating method. VGCF has been added to improve the adherence of the micro-porous layer to the macro-porous layer. Fig. 6 shows typical surface morphology of the wire rod coated micro-porous layer of the GDL, showing crack free surface. Recent developments in the preparation of GDL by wet slurry rather than dry methods would help mass production of GDL with less environmental concerns [302,303]. Alternatively the preparation of GDL with catalyst paste has also been reported [304]. The hydrophobic properties of carbon fibers improved by a CF4 plasma treatment has been used to fabricate GDL [305]. Ultralow loading noble metal (Pt) electrodes were reported via dual ion-beam assisted deposition of pure Pt metal particles directly onto the surface of a noncatalyzed E-TEK's GDL [306–308]. Adding a micro-porous layer to traditional GDL can enhance the ability of water management, and therefore achieve better cell performance and higher current density. The Vulcan XC-72R carbon loading of 1 mg cm^{-2} in the micro-porous layer has been reported by Yan et al. [309] for the high performance. Feasibility and the effects of design parameters have been examined for micromachined metallic thin film GDL for PEMFCs [310]. With the titanium thin film impact of design parameters such as through-hole diameter, through-hole patterning and the thin film thickness have been investigated to show the parameter dependence and design optimization. Porous film structure for an electrode GDL has been reported [311]. High conductivity of GDL film, using low-viscosity polypropylene and polystyrene as the two immiscible polymer components of the film and the conductive additives composed of high specific surface area carbon black and synthetic flake graphite filling the film matrix, has been prepared and tested. A micro-porous layer of a triple-layer gas diffusion electrode for a PEMFC has been made by a dispersion of carbon black and PTFE particles using a non-ionic surfactant such as Triton X-100 and reported [312]. A review on the compositions, present fabrication processes and properties of GDL along with the development trends, has been presented by Wang et al. [313].

5. Manufacture

The introduction of fuel cell technologies into the market is determined by the offering price reduction of components. Currently, there are very few Commercial GDL manufactures in the market. There are three international manufacturers such as SGL Technologies GmbH, Mitsubishi Rayon Co., Ltd., Japan, and Ballard Material Products, Inc., Lowell, Massachusetts. Cost and functional quality are the points of most concern in GDL manufacture for PEMFC technology. GDL has been based on carbon or graphite fiber. These materials are very costly and are of very limited design flexibility. They also cause the fiber penetration through the polymer electrolyte membrane. To solve these problems, significant efforts are being made by researchers to find the best alternative materials. In fact the cost of the GDLs within the membrane–electrode constitutes about 20% and about 5% of the overall fuel cell stack. Hence the cost of GDLs also plays a critical role in reducing the fuel cell system cost for early commercialization.

6. Conclusion

GDL is an essential component of PEMFC. The choice of materials for GDL will depend on the required multi-functionality of its structure. As the best components for each of the functionality cannot make the best GDL, a trade-off between the properties will evolve the optimum GDL. Hence factors such as electronic resistivity, fraction of hydrophobic pores, gas permeability, pore size distribution and the surface morphology, will define the functionality of the GDL as the electronic resistivity of a dual-layer. GDL is dependent on the macro-porous substrate and its gas permeability which is related to larger pores and water management which relies on the fraction of hydrophobic pores. A significant technical challenge in a PEMFC is that the fuel cell is prone to excess liquid water formation due to water production from the oxygen reduction reaction at the cathode. Hence development of highly functionalised GDL with self-adjusting characteristics of water retention and water draining, along with the structural features to steadily supply the reactant gases to the catalyst layer will be essential for the mass utilization of fuel cells for various power density applications.

References

[1] M. Mathias, J. Roth, J. Fleming, W. Lehnert, in: W. Vielstich, A. Lamm, H.A. Gasteiger (Eds.), Handbook of Fuel Cells: Fundamentals, Technology, Applications, Wiley, 2003, pp. 46.1–46.21.
[2] G. Hoogers, in: G. Hoogers (Ed.), Fuel Cell Technology Handbook, CRC Press LLC, 2003, pp. 4.1–4.27.
[3] B. Du, Q. Guo, Z. Qi, L. Mao, R. Pollard, J.F. Elter, in: R.H. Jones, G.J. Thomas (Eds.), Materials for Hydrogen Economy, CRC Press, 2007, pp. 251–310.
[4] L.R. Jordan, A.K. Shukla, T. Behrsing, N.R. Avery, B.C. Muddle, M. Forsyth, J. Appl. Electrochem. 30 (2000) 641–646.
[5] M. Neergat, A.K. Shukla, J. Power Sources 104 (2002) 289–294.
[6] C. Lim, C.Y. Wang, Electrochim. Acta 49 (2004) 4149–4156.
[7] G.G. Park, Y.J. Sohn, T.H. Yang, Y.G. Yoon, W.Y. Lee, C.S. Kim, J. Power Sources 131 (2002) 182–187.
[8] G.Y. Lin, T.V. Nguyen, J. Electrochem. Soc. 152 (2005) A1942–A1948.
[9] H. Nakajima, T. Konomi, T. Kitahara, J. Power Sources 171 (2007) 457–463.
[10] S. Park, J.W. Lee, B.N. Popov, J. Power Sources 177 (2008) 457–463.
[11] E.D. Wang, P.F. Shi, C.Y. Du, Electrochem. Commun. 10 (2008) 555–558.
[12] J.T. Gostick, M.W. Fowler, M.A. Ioannidis, M.D. Pritzker, Y.M. Volfkovich, A. Sakars, J. Power Sources 156 (2006) 375–387.
[13] L.R. Jordan, A.K. Shukla, T. Behrsing, N.R. Avery, B.C. Muddle, M. Forsyth, J. Power Sources 86 (2000) 250–254.
[14] U. Pasaogullari, C.Y. Wang, Electrochim. Acta 49 (2004) 4359–4369.
[15] H.K. Lee, J.H. Park, D.Y. Kim, T.H. Lee, J. Power Sources 131 (2004) 200–206.
[16] A.M. Kannan, P. Kanagala, V. Veedu, J. Power Sources (2009), doi:10.1016/j.jpowsour.2009.03.022.
[17] M.V. Williams, E. Begg, L. Bonville, H.R. Kunz, J.M. Fentona, J. Electrochem. Soc. 151 (2004) A1173–A1180.

[18] A.Z. Weber, J. Newman, J. Electrochem. Soc. 152 (2005) A677–A688.
[19] W.M. Yan, C.Y. Soong, F.L. Chen, H.S. Chu, J. Power Sources 125 (2004) 27–39.
[20] X.L. Wang, H.M. Zhang, J.L. Zhang, H.F. Xu, Z.Q. Tian, J. Chen, H.X. Zhong, Y.M. Liang, B.L. Yi, Electrochim. Acta 51 (2006) 4909–4915.
[21] R. Roshandel, B. Farhanieh, E. Saievar-Iranizad, Renew. Energy 30 (2005) 1557–1572.
[22] X.L. Wang, H.M. Zhang, J.L. Zhang, H.F. Xu, X.B. Zhu, J. Chen, B.L. Yi, J. Power Sources 162 (2006) 474–479.
[23] Z.G. Zhan, J.S. Xiao, D.Y. Li, M. Pan, R.Z. Yuan, J. Power Sources 160 (2006) 1041–1048.
[24] J.I. Gostick, M.A. Ioannidis, M.W. Fowler, M.D. Pritzker, J. Power Sources 173 (2007) 277–290.
[25] S. Park, J.W. Lee, B.N. Popov, J. Power Sources 163 (2006) 357–363.
[26] H.L. Tang, S.L. Wang, M. Pan, R.Z. Yuan, J. Power Sources 166 (2007) 41–46.
[27] Z.G. Zhan, J.S. Xiao, Y.S. Zhang, M. Pan, R.Z. Yuan, Int. J. Hydrogen Energy 32 (2007) 4443–4451.
[28] H.K. Atiyeh, K. Karan, B. Peppley, A. Phoenix, E. Halliop, J. Pharoah, J. Power Sources 170 (2007) 111–121.
[29] A.M. Kannan, L. Cindrella, L. Munukutla, Electrochim. Acta 53 (2008) 2416–2422.
[30] F.L. Chen, M.H. Chang, P.T. Hsieh, Int. J. Hydrogen Energy 33 (2008) 2525–2529.
[31] M. Han, J.H. Xu, S.H. Chan, S.P. Jiang, Electrochim. Acta 53 (2008) 5361–5367.
[32] G. Selvarani, A.K. Sahu, P. Sridhar, S. Pitchumani, A.K. Shukla, J. Appl. Electrochem. 38 (2008) 357–362.
[33] Y. Deyrail, F. Mighri, M. Bousmina, S. Kaliaguine, Fuel Cells 7 (2007) 447–452.
[34] V. Gurau, M.J. Bluemle, E.S. De Castro, Y.M. Tsou, T.A. Zawodzinski Jr., J. Adin Mann Jr., J. Power Sources 165 (2007) 793–802.
[35] J.P. Feser, A.K. Prasad, S.G. Advani, J. Power Sources 162 (2006) 1226–1231.
[36] W. Sun, B.A. Peppley, K. Karan, J. Power Sources 144 (2005) 42–53.
[37] J.T. Gostick, M.W. Fowler, M.D. Pritzker, M.A. Ioannidis, L.M. Behra, J. Power Sources 162 (2006) 228–238.
[38] Y. Shi, J.S. Xiao, M. Pan, R.Z. Yuan, J. Power Sources 160 (2006) 277–283.
[39] Y. Shi, J.S. Xiao, M. Pan, R.Z. Yuan, J. WuHan Univ. Technol. Mater. Sci. Ed. 21 (2006) 22–25.
[40] G. Inoue, Y. Matsukuma, M. Minemoto, J. Power Sources 157 (2006) 153–165.
[41] G.L. He, Z.C. Zhao, P.W. Ming, A. Abuliti, C.Y. Yin, J. Power Sources 163 (2007) 846–852.
[42] J. Zou, X.F. Peng, W.M. Yan, J. Power Sources 159 (2006) 514–523.
[43] Z.Y. Shi, X. Wang, J. Power Sources 185 (2008) 985–992.
[44] U. Pasaogullari, C.Y. Wang, J. Electrochem. Soc. 151 (2004) A399–A406.
[45] X.G. Yang, F.Y. Zhang, A.L. Lubawy, C.Y. Wang, Electrochem. Solid State Lett. 7 (2004) A408–A411.
[46] M. Wohr, K. Bolwin, W. Schnurnberger, M. Fischer, W. Neubrand, G. Eigenberger, Int. J. Hydrogen Energy 23 (1998) 213–218.
[47] Y.W. Rho, S. Srinivasan, Y.T. Kho, J. Electrochem. Soc. 141 (1994) 2089–2096.
[48] D. Kramer, J.B. Zhang, R. Shimoi, E. Lehmann, A. Wokaun, K. Shinohara, G.G. Scherer, Electrochim. Acta 50 (2005) 2603–2614.
[49] Y. Wang, C.Y. Wang, Electrochim. Acta 50 (2005) 1307–1315.
[50] D. Natarajan, T.V. Nguyen, J. Electrochem. Soc. 148 (2001) A1324–A1335.
[51] S. Litster, D. Sinton, N. Djilali, J. Power Sources 154 (2006) 95–105.
[52] J.B. Zhang, D. Kramer, R. Shimoi, Y. Ona, E. Lehmann, A. Wokaun, K. Shinohara, G.G. Scherer, Electrochim. Acta 51 (2006) 2715–2727.
[53] Y. Wang, C.Y. Wang, J. Electrochem. Soc. 153 (2006) A1193–A1200.
[54] U. Pasaogullari, C.Y. Wang, K.S. Chen, J. Electrochem. Soc. 152 (2005) A1574–A1582.
[55] G.Y. Lin, T.V. Nguyen, J. Electrochem. Soc. 153 (2006) A372–A382.
[56] J.J. Hwang, C.K. Chen, R.F. Savinell, C.C. Liu, J. Wainright, J. Appl. Electrochem. 34 (2004) 217–224.
[57] S.W. Cha, R. O'Hayre, Y. Saito, F.B. Prinz, J. Power Sources 134 (2004) 57–71.
[58] K.T. Jeng, S.F. Lee, G.F. Tsai, C.H. Wang, J. Power Sources 138 (2004) 41–50.
[59] E.C. Kumbur, K.V. Sharp, M.M. Mench, J. Power Sources 161 (2006) 333–345.
[60] P.K. Sinha, P. Halleck, C.Y. Wang, Electrochem. Solid State Lett. 9 (2006) A344–A348.
[61] Y. Wang, C.Y. Wang, J. Power Sources 147 (2005) 148–161.
[62] J.P. Owejan, T.A. Trabold, D.L. Jacobson, D.R. Baker, D.S. Hussey, M. Arif, Int. J. Heat Mass Transf. 49 (2006) 4721–4731.
[63] V. Gurau, M.J. Bluemle, E.S. De Castro, Y.M. Tsou, J.A. Mann, T.A. Zawodzinski, J. Power Sources 160 (2006) 1156–1162.
[64] T. Mennola, M. Noponen, M. Aronniemi, T. Hottinen, M. Mikkola, O. Himanen, P. Lund, J. Appl. Electrochem. 33 (2003) 979–987.
[65] S. Litster, J.G. Pharoah, G. McLean, N. Djilali, J. Power Sources 156 (2006) 334–344.
[66] C.Y. Soong, W.M. Yan, C.Y. Tseng, H.C. Liu, F.L. Chen, H.S. Chu, J. Power Sources 143 (2005) 36–47.
[67] A. Theodorakakos, T. Ous, A. Gavaises, J.M. Nouri, N. Nikolopoulos, H. Yanagihara, J. Colloid Interface Sci. 300 (2006) 673–687.
[68] J.G. Pharoah, K. Karan, W. Sun, J. Power Sources 161 (2006) 214–224.
[69] S.U. Jeong, E.A. Cho, H.J. Kim, T.H. Lim, I.H. Oh, S.H. Kim, J. Power Sources 159 (2006) 1089–1094.
[70] Y. Wang, C.Y. Wang, J. Electrochem. Soc. 154 (2007) B636–B643.
[71] A. Kazim, P. Forges, H.T. Liu, Int. J. Energy Res. 27 (2003) 401–414.
[72] Q.Z. Guo, V.A. Sethuraman, R.E. White, J. Electrochem. Soc. 151 (2004) A983–A993.
[73] J.P. Feser, A.K. Prasad, S.G. Advani, J. Power Sources 161 (2006) 404–412.
[74] D.T. Song, Q.P. Wang, Z.S. Liu, C. Huang, J. Power Sources 159 (2006) 928–942.
[75] Y. Bultel, K. Wiezell, F. Jaouen, P. Ozil, G. Lindbergh, Electrochim. Acta 51 (2005) 474–488.
[76] P.K. Sinha, C.Y. Wang, Electrochim. Acta 52 (2007) 7936–7945.
[77] L. Sun, P.H. Oosthuizen, K.B. McAuley, Int. J. Therm. Sci. 45 (2006) 1021–1026.
[78] K. Promislow, J. Stockie, B. Wetton, Proc. R. Soc. A Math. Phys. Eng. Sci. 462 (2006) 789–816.
[79] J.M. Song, H. Uchida, M. Watanabe, Electrochemistry 73 (2005) 189–193.
[80] H.T. Liu, T.H. Zhou, J. Enhanc. Heat Transf. 10 (2003) 257–274.
[81] D.S. Hussey, D.L. Jacobson, M. Arif, J.P. Owejan, J.J. Gagliardo, T.A. Trabold, J. Power Sources 172 (2007) 225–228.
[82] J. Park, X.G. Li, J. Power Sources 163 (2007) 853–863.
[83] J.D. Fairweather, P. Cheung, J. St-Pierre, D.T. Schwartz, Electrochem. Commun. 9 (2007) 2340–2345.
[84] G.L. He, P.W. Ming, Z.C. Zhao, A. Abudula, Y. Xiao, J. Power Sources 163 (2007) 864–873.
[85] Z.X. Liu, Z.Q. Mao, C. Wang, J. Power Sources 158 (2006) 1229–1239.
[86] H.C. Liu, W.M. Yan, X.D. Wang, J. Electrochem. Soc. 154 (2007) B1338–B1348.
[87] B. Markicevic, A. Bazylak, N. Djilali, J. Power Sources 171 (2007) 706–717.
[88] M. Vynnycky, Appl. Math. Comp. 189 (2007) 1560–1575.
[89] A.Z. Weber, R.M. Darling, J. Power Sources 168 (2007) 191–199.
[90] T. Koido, T. Furusawa, K. Moriyama, J. Power Sources 175 (2008) 127–136.
[91] H. Meng, J. Power Sources 161 (2006) 466–469.
[92] Z.G. Zhan, J.S. Xiao, M. Pan, R.Z. Yuan, J. Power Sources 160 (2006) 1–9.
[93] M.H. Chang, F.L. Chen, H.S. Teng, J. Power Sources 160 (2006) 268–276.
[94] V. Gurau, T.A. Zawodzinski, J.A. Mann, J. Fuel Cell Sci. Technol. 5 (2008) 21009–21021.
[95] K. Yoshizawa, K. Ikezoe, Y. Thsaki, D. Kramer, E.H. Lehmann, G.G. Scherer, J. Electrochem. Soc. 155 (2008) B223–B227.
[96] M. Al-Baghdadi, H. Al-Janabi, Energy Convers. Manage. 48 (2007) 3102–3119.
[97] M. Al-Baghdadi, H. Al-Janabi, J. Power Energy 221 (2007) 941–953.
[98] J.J. Hwang, C.H. Chao, W. Wu, J. Power Sources 163 (2006) 450–459.
[99] C.R. Tsai, F.L. Chen, A.C. Ruo, M.H. Chang, H.S. Chu, C.Y. Soong, W.M. Yan, C.H. Cheng, J. Power Sources 160 (2006) 50–56.
[100] M.S. Chiang, H.S. Chu, J. Power Sources 160 (2006) 340–352.
[101] J.H. Jang, W.M. Yan, C.C. Shih, J. Power Sources 156 (2006) 244–252.
[102] J.G. Pharoah, Int. J. Green Energy 2 (2005) 421–438.
[103] M.G. Hu, X.J. Zhu, A.Z. Gu, Chin. J. Chem. Eng. 12 (2004) 14–26.
[104] K. Promislow, P. Chang, B. Haas, H. Wetton, J. Electrochem. Soc. 155 (2008) A494–A504.
[105] O. Chapuis, M. Prat, M. Quintard, E. Chane-Kane, O. Guillot, N. Mayer, J. Power Sources 178 (2008) 258–268.
[106] D. Gerteisen, T. Heilmann, C. Ziegler, J. Power Sources 177 (2008) 348–354.
[107] C. Ziegler, T. Heilmann, D. Gerteisen, J. Electrochem. Soc. 155 (2008) B349–B355.
[108] M.A. Hickner, N.P. Siegel, K.S. Chen, D.S. Hussey, D.L. Jacobson, M. Arif, J. Electrochem. Soc. 155 (2008) B427–B434.
[109] P.K. Sinha, C.Y. Wang, Chem. Eng. Sci. 63 (2008) 1081–1091.
[110] A. Bazylak, D. Sinton, N. Djilali, J. Power Sources 176 (2008) 240–246.
[111] P.H. Lee, S.A. Cho, S.S. Han, S.S. Hwang, Int. J. Automotive Technol. 8 (2007) 761–769.
[112] T. Ous, C. Arcoumanis, J. Power Sources 173 (2007) 137–148.
[113] J. Park, M. Matsubara, X. Li, J. Power Sources 173 (2007) 404–414.
[114] X.D. Niu, T. Munekata, S.A. Hyodo, K. Suga, J. Power Sources 172 (2007) 542–552.
[115] M. Al-Baghdadi, H. Al-Janabi, J. Zhenjiang Univ. Sci. A 8 (2007) 285–300.
[116] W.M. Yan, H.S. Chu, J.Y. Chen, C.Y. Soong, F.L. Chen, J. Power Sources 162 (2006) 1147–1156.
[117] S.A. Grigoriev, A.A. Kalinnikov, V.N. Fateev, A.A. Wragg, J. Appl. Electrochem. 36 (2006) 991–996.
[118] J.T. Gostick, M.A. Ioannidis, M.W. Fowler, M.D. Pritzker, Electrochem. Commun. 10 (2008) 1520–1523.
[119] K. Jiao, B. Zhou, J. Fuel Cell Sci. Technol. 5 (2008) 41011–41021.
[120] A. Bazylak, V. Berejnov, B. Markicevic, D. Sinton, N. Djilali, Electrochim. Acta 53 (2008) 7630–7637.
[121] M.K. Baboh, M.J. Kermani, Electrochim. Acta 53 (2008) 7644–7654.
[122] X.H. Wang, T.V. Nguyen, J. Electrochem. Soc. 155 (2008) B1085–B1092.
[123] D.H. Ahmed, H.J. Sung, J. Bae, Int. J. Hydrogen Energy 33 (2008) 3786–3800.
[124] C. Siegel, Energy 33 (2008) 1331–1352.
[125] J. Park, X.Q. Li, D. Tran, T. Abdel-Baset, D.S. Hussey, D.L. Jacobson, M. Arif, Int. J. Hydrogen Energy 33 (2008) 3373–3384.
[126] P. Jain, L.T. Biegler, M.S. Jhon, Electrochem. Solid State Lett. 11 (2008) B193–B196.
[127] J. Chen, H.F. Xu, H.M. Zhang, B.L. Yi, J. Power Sources 182 (2008) 531–539.
[128] T. Mukaide, S. Mogi, J. Yamamoto, A. Morita, S. Koji, K. Takada, K. Uesugi, K. Kajiwara, T. Noma, J. Synchrotron Radiat. 15 (2008) 329–334, Part 4.
[129] X. Zhu, P.C. Sui, N. Djilali, J. Power Sources 181 (2008) 101–115.
[130] T. Ha, B. Kim, H.S. Kim, K. Min, J. Mech. Sci. Technol. 22 (2008) 1030–1036.
[131] X. Zhu, P.C. Sui, N. Djilali, Microfluid. Nanofluid. 4 (2008) 543–555.
[132] E.C. Kumbur, K.V. Sharp, M.M. Mench, J. Power Sources 176 (2008) 191–199.
[133] J.P. Feser, A.K. Prasad, S.G. Advani, J. Fuel Cell Sci. Technol. 4 (2007) 328–335.
[134] T. Fabian, R. O'Hayre, F.B. Prinz, J.G. Santiago, J. Electrochem. Soc. 154 (2007) B910–B918.
[135] K. Promislow, J.M. Stockie, Siam. J. Appl. Math. 62 (2001) 180–205.
[136] Y.G. Chirkov, V.I. Rostokin, Russ. J. Electrochem. 44 (2008) 910–920.
[137] P. Mocoteguy, F. Druart, Y. Bultel, S. Besse, A. Rakotondrainibe, J. Power Sources 167 (2007) 349–357.

[138] K. Nishida, S. Tsushima, K. Teranishi, S. Hirai, Kagaku Kogaku Ronbunshu 33 (2007) 181–185.
[139] K. Nishida, T. Murakami, S. Tsushima, S. Hirai, Electrochemistry 75 (2007) 149–151.
[140] P.K. Sinha, P.P. Mukherjee, C.Y. Wang, J. Mater. Chem. 17 (2007) 3089–3103.
[141] R. Satija, D.L. Jacobson, M. Arif, S.A. Werner, J. Power Sources 129 (2004) 238–245.
[142] F.Y. Zhang, X.G. Yang, C.Y. Wang, J. Electrochem. Soc. 153 (2006) A225–A232.
[143] U. Pasaogullari, C.Y. Wang, J. Electrochem. Soc. 152 (2005) A380–A390.
[144] H. Meng, C.Y. Wang, J. Electrochem. Soc. 152 (2005) A1733–A1741.
[145] G.Y. Lin, W.S. He, T.V. Nguyen, J. Electrochem. Soc. 151 (2004) A1999–A2006.
[146] J. Chen, T. Matsuura, M. Hori, J. Power Sources 131 (2004) 155–161.
[147] M.V. Williams, H.R. Kunz, J.M. Fenton, J. Power Sources 135 (2004) 122–134.
[148] J. Benziger, J. Nehlsen, D. Blackwell, T. Brennan, J. Itescu, J. Membr. Sci. 261 (2005) 98–106.
[149] P. Staiti, Z. Poltarzewski, V. Alderucci, G. Maggio, N. Giordano, A. Fasulo, J. Appl. Electrochem. 22 (1992) 663–667.
[150] J.B. Hou, H.M. Yu, S.S. Zhang, S.C. Sun, H.W. Wang, B.L. Yi, P.W. Ming, J. Power Sources 162 (2006) 513–520.
[151] S.H. Ge, C.Y. Wang, Electrochem. Solid State Lett. 9 (2006) A499–A503.
[152] M. Oszcipok, M. Zedda, D. Riemann, D. Geckeler, J. Power Sources 154 (2006) 404–411.
[153] K.S. Chen, M.A. Hickner, D.R. Noble, Int. J. Energy Res. 29 (2005) 1113–1132.
[154] K. Sugiura, M. Nakata, T. Yodo, Y. Nishiguchi, M. Yamauchi, Y. Itoh, J. Power Sources 145 (2005) 526–533.
[155] Q.G. Yan, H. Toghiani, Y.W. Lee, K.W. Liang, H. Causey, J. Power Sources 160 (2006) 1242–1250.
[156] L. Mao, C.Y. Wang, Y. Tabuchi, J. Electrochem. Soc. 154 (2007) B341–B351.
[157] V.P. Schulz, J. Becker, A. Wiegmann, P.P. Mukherjee, C.Y. Wang, J. Electrochem. Soc. Y 154 (2007) B419–B426.
[158] T. Fabian, J.D. Posner, R. O'Hayre, S.W. Cha, J.K. Eaton, F.B. Prinz, J.G. Santiago, J. Power Sources 161 (2006) 168–182.
[159] C.R. Buie, J.D. Posner, T. Fabian, C.A. Suk-Won, D. Kim, F.B. Prinz, J.K. Eaton, J.G. Santiago, J. Power Sources 161 (2006) 191–202.
[160] B. Thoben, A. Siebke, J. New Mater. Electrochem. Syst. 7 (2004) 13–20.
[161] D. Spernjak, A.K. Prasad, S.G. Advani, J. Power Sources 170 (2007) 334–344.
[162] Y. Wang, C.Y. Wang, K.S. Chen, Electrochim. Acta 52 (2007) 3965–3975.
[163] R.K. Ahluwalia, X. Wang, J. Power Sources 162 (2006) 502–512.
[164] W.H.J. Hogarth, J.B. Benziger, J. Power Sources 159 (2006) 968–978.
[165] Q.Z. Guo, R.E. White, J. Electrochem. Soc. 151 (2004) E133–E149.
[166] S. Ge, C.Y. Wang, J. Electrochem. Soc. 154 (2007) B998–B1005.
[167] S. Litster, C.R. Buie, T. Fabian, J.K. Eaton, J.G. Santiago, J. Electrochem. Soc. 154 (2007) B1049–B1058.
[168] K. Jiao, B. Zhou, J. Power Sources 169 (2007) 296–314.
[169] E.C. Kumbur, K.V. Sharp, M.M. Mench, J. Power Sources 168 (2007) 356–368.
[170] X. Zhu, P.C. Sui, N. Djilali, J. Power Sources 172 (2007) 287–295.
[171] C. Lee, W. Merida, J. Power Sources 164 (2007) 141–153.
[172] C.I. Lee, H.S. Chu, J. Power Sources 161 (2006) 949–956.
[173] H. Yamada, T. Hatanaka, H. Murata, Y. Morimoto, J. Electrochem. Soc. 153 (2006) A1748–A1754.
[174] H. Li, Y.H. Tang, Z.W. Wang, Z. Shi, S.H. Wu, D.T. Song, J.L. Zhang, K. Fatih, J.J. Zhang, H.J. Wang, Z.S. Liu, R. Abouatallah, A. Mazza, J. Power Sources 178 (2008) 103–117.
[175] U. Pasaogullari, P.P. Mukherjee, C.Y. Wang, K.S. Chen, J. Electrochem. Soc. 154 (2007) B823–B834.
[176] L.J. Bonville, H.R. Kunz, Y. Song, A. Mientek, M. Williams, A. Ching, J.M. Fenton, J. Power Sources 144 (2005) 107–112.
[177] J.P. Owejan, T.A. Trabold, J. Gagliardo, D.L. Jacobson, R.N. Carter, D.S. Hussey, M. Arif, J. Power Sources 171 (2007) 626–633.
[178] S. Shimpalee, U. Beuscher, J.W. Van Zee, Electrochim. Acta 52 (2007) 6748–6754.
[179] P. Quan, M.C. Lai, J. Power Sources 164 (2007) 222–237.
[180] J.B. Hou, B.L. Yi, H.M. Yu, L.X. Hao, W. Song, Y. Fu, Z.G. Shao, Int. J. Hydrogen Energy 32 (2007) 4503–4509.
[181] G. Inoue, T. Yoshimoto, Y. Matsukuma, M. Minemoto, H. Itoh, S. Tsurumaki, J. Power Sources 162 (2006) 81–93.
[182] S. Vengatesan, H.J. Kim, E.A. Cho, S.U. Jeong, H.Y. Ha, I.H. Oh, S.A. Hong, T.H. Lim, J. Power Sources 156 (2006) 294–299.
[183] Y. Ishikawa, H. Harnada, M. Uehara, M. Shiozawa, J. Power Sources 179 (2008) 547–552.
[184] P.K. Sinha, C.Y. Wang, J. Electrochem. Soc. 154 (2007) B1158–B1166.
[185] H. Wu, X.G. Li, P. Berg, Int. J. Hydrogen Energy 32 (2007) 2022–2031.
[186] D.H. Ahmed, H.J. Sung, Int. J. Heat Mass Transf. 50 (2007) 3376–3389.
[187] K.W. Feindel, S.H. Bergens, R.E. Wasylishen, PCCP 9 (2007) 1850–1857.
[188] E.S.J. Chia, J.B. Benziger, L.G. Kevrekidis, AIChE J. 52 (2006) 3902–3910.
[189] Y. Yoshikawa, T. Matsuura, M. Kato, M. Hori, J. Power Sources 158 (2006) 143–147.
[190] P. Schott, P. Baurens, J. Power Sources 156 (2006) 85–91.
[191] N. Holmstrom, J. Ihonen, A. Lundblad, G. Lindbergh, Fuel Cells 7 (2007) 306–313.
[192] Q. Liu, J. Wu, J. Fuel Cell Sci. Technol. 3 (2006) 51–61.
[193] L.B. Wang, N.I. Wakayama, T. Okada, Iron Steel Inst. Jpn. Int. 45 (2005) 1005–1013.
[194] W.W. Yang, T.S. Zhao, Y.L. He, J. Power Sources 185 (2008) 765–775.
[195] S.J. Lee, N.J. Lim, S. Kim, G.G. Park, C.S. Kim, J. Power Sources 185 (2008) 867–870.
[196] A. Bazylak, J. Heinrich, N. Djilali, D. Sinton, J. Power Sources 185 (2008) 1147–1153.
[197] Y.S. Chen, H. Peng, J. Power Sources 185 (2008) 1179–1192.
[198] W. Dai, H.J. Wang, X.Z. Yuan, J.J. Martin, Z.P. Luo, M. Pan, J. Power Sources 185 (2008) 1267–1271.
[199] C. Hartnig, R. Kuhn, P. Kruger, I. Manke, N. Kardjilov, J. Goebbels, B.P. Muller, H. Riesemeier, MP Mater. Test. Mater. Compon. Technol. Appl. 50 (2008) 609–614.
[200] H. Meng, Int. J. Hydrogen Energy 33 (2008) 5738–5747.
[201] S.K. Roy, M.E. Orazem, J. Power Sources 184 (2008) 212–219.
[202] J.B. Siegel, D.A. Mckay, A.G. Stefanopoulou, D.S. Hussey, D.L. Jacobson, J. Electrochem. Soc. 155 (2008) B1168–B1178.
[203] J. Hermann, C. Ziegler, J. Electrochem. Soc. 155 (2008) B1066–B1076.
[204] D.H. Ahmed, H.J. Sung, J. Bae, Int. J. Hydrogen Energy 33 (2008) 3767–3785.
[205] R.P. Ramasamy, E.C. Kumbur, M.M. Mench, W. Liu, D. Moore, M. Murthy, Int. J. Hydrogen Energy 33 (2007) 3351–3367.
[206] W.Y. Shi, E. Kurihara, N. Oshima, J. Power Sources 182 (2008) 112–118.
[207] S.G. Kandlikar, Heat Transf. Eng. 29 (2008) 575–587.
[208] M. Naijari, F. Khernili, S. Ben Nasrallah, Renew. Energy 33 (2008) 1824–1831.
[209] T. Metz, N. Paust, C. Mfiller, R. Zengerle, P. Koltay, Sens. Actuators A: Phys. 143 (2008) 49–57.
[210] D.H. Ahmed, H.J. Sung, J. Bae, D.R. Lee, Int. J. Heat Mass Transf. 51 (2008) 2006–2019.
[211] J. Park, X. Li, J. Power Sources 178 (2008) 248–257.
[212] H. Masuda, K. Ito, T. Oshima, K. Sasaki, J. Power Sources 177 (2008) 303–313.
[213] K. Ito, K. Ashikaga, H. Masuda, T. Oshima, Y. Kakimoto, K. Sasaki, J. Power Sources 175 (2008) 732–738.
[214] I.E. Baranov, S.A. Grigor'ev, I.I. Nikolaev, V.N. Fateev, Russ. J. Electrochem. 42 (2006) 1325–1331.
[215] C.H. Yun, Y.C. Chung, S.C. Yi, J. Ceram. Process. Res. 7 (2006) 245–252.
[216] H. Meng, C.Y. Wang, J. Electrochem. Soc. 151 (2004) A358–A367.
[217] M.M. Mench, C.Y. Wang, M. Ishikawa, J. Electrochem. Soc. 150 (2003) A1052–A1059.
[218] M. Noponen, T. Mennola, M. Mikkola, T. Hottinen, P. Lund, J. Power Sources 106 (2006) 304–312.
[219] W.K. Lee, S. Shimpalee, J.W. Van Zee, J. Electrochem. Soc. 150 (2003) A341–A348.
[220] V. Mishra, F. Yang, R. Pitchumani, J. Fuel Cell Sci. Technol. (2004) 2–9.
[221] M. Noponen, J. Ihonen, A. Lundblad, G. Lindbergh, J. Appl. Electrochem. 34 (2004) 255–262.
[222] D. Natarajan, T.V. Nguyen, J. Power Sources 135 (2004) 95–109.
[223] L.H. Zhang, Y. Liu, H.M. Song, S.X. Wang, Y.Y. Zhou, S.J. Hu, J. Power Sources 162 (2006) 1165–1171.
[224] P.C. Sui, N. Djilali, J. Power Sources 161 (2006) 294–300.
[225] H. Sun, G.S. Zhang, L.J. Guo, H.T. Liu, J. Power Sources 158 (2006) 326–332.
[226] S.A. Freunberger, M. Reum, J. Evertz, A. Wokaun, F.N. Buchi, J. Electrochem. Soc. 153 (2006) A2158–A2165.
[227] Y. Zhou, G. Lin, A.J. Shih, S.J. Hu, J. Power Sources 163 (2007) 777–783.
[228] I. Nitta, O. Himanen, M. Mikkola, Electrochem. Commun. 10 (2008) 47–51.
[229] L. Wang, H.T. Liu, J. Power Sources 180 (2008) 365–372.
[230] Y.G. Chirkov, V.I. Rostokin, Russ. J. Electrochem. 43 (2007) 25–33.
[231] I. Onda, T. Araki, T. Taniuchi, D. Sunakawa, K. Wakahara, M. Nagahama, J. Electrochem. Soc. 154 (2007) B247–B257.
[232] M. Barber, T.S. Sun, E. Petrach, X. Wang, Q. Zou, J. Power Sources 185 (2008) 1252–1256.
[233] A.P. Suvorov, J. Elter, R. Staudt, R. Hamm, G.J. Tudryn, L. Schadler, G. Eisman, Int. J. Solids Struct. 45 (2008) 5987–6000.
[234] C.J. Bapat, S.T. Thynell, J. Power Sources 185 (2008) 428–432.
[235] F.N. Buchi, M. Reum, Meas. Sci. Technol. 19 (2008) 85702–85708.
[236] X.M. Lai, D.A. Liu, L.F. Peng, J. Ni, J. Power Sources 182 (2008) 153–159.
[237] Z.L. Wu, Y.Y. Zhou, G.S. Lin, S.X. Wang, S.J. Hu, J. Power Sources 182 (2008) 265–269.
[238] I. Li, C.Y. Wang, A. Su, J. Electrochem. Soc. 155 (2008) B64–B69.
[239] L.K. Kwac, H.G. Kim, J. Mech. Sci. Technol. 22 (2008) 1561–1567.
[240] Z.G. Qi, A. Kaufman, J. Power Sources 109 (2002) 38–46.
[241] J.M. Song, S.Y. Cha, W.M. Lee, J. Power Sources 94 (2001) 78–84.
[242] I. Giorgi, E. Antolini, A. Pozio, E. Passalacqua, Electrochim. Acta 43 (1998) 3675–3680.
[243] J. Moreira, A.L. Ocampo, P.J. Sebastian, A.S. Mascha, M.D. Salazar, P. del Angel, J.A. Montoya, R. Pérez, L. Martínez, Int. J. Hydrogen Energy 28 (2003) 625–627.
[244] A.M. Kannan, A. Menghal, I. Barsukov, Electrochem. Commun. 8 (2006) 887–891.
[245] A.M. Kannan, V.P. Veedu, L. Munukutla, M.N. Ghasemi-Nejhad, Electrochem. Solid State Lett. 10 (2007) B47–B50.
[246] J.B. Ge, A. Higier, H.T. Liu, J. Power Sources 159 (2006) 922–927.
[247] A. Bazylak, D. Sinton, Z.S. Liu, N. Djilali, J. Power Sources 163 (2007) 784–792.
[248] S. Escribano, J.F. Blachot, M. Etheve, A. Morin, R. Mosdale, J. Power Sources 156 (2006) 8–13.
[249] I. Nitta, T. Hottinen, O. Himanen, M. Mikkola, J. Power Sources 171 (2007) 26–36.
[250] P. Zhou, C.W. Wu, G.J. Ma, J. Power Sources 163 (2007) 874–881.
[251] P. Zhou, C.W. Wu, G.J. Ma, J. Power Sources 159 (2006) 1115–1122.
[252] S.J. Lee, C.D. Hsu, C.H. Huang, J. Power Sources 145 (2005) 353–361.
[253] T. Hottinen, O. Himanen, S. Karvonen, I. Nitta, J. Power Sources 171 (2007) 113–121.
[254] P. Zhou, C.W. Wu, J. Power Sources 170 (2007) 93–100.

[255] W.R. Chang, J.J. Hwang, F.B. Weng, S.H. Chan, J. Power Sources 166 (2007) 149–154.
[256] T. Hottinen, O. Himanen, Electrochem. Commun. 9 (2007) 1047–1052.
[257] Z.Y. Su, C.T. Liu, H.P. Chang, C.H. Li, K.J. Huang, P.C. Sui, J. Power Sources 183 (2008) 182–192.
[258] J.H. Lin, W.H. Chen, Y.J. Su, T.H. Ko, Fuel 87 (2008) 2420–2424.
[259] I. Nitta, O. Himanen, M. Mikkola, Fuel Cells 8 (2008) 111–119.
[260] S.Y. Lee, K.S. Lee, S. Um, J. Mech. Sci. Technol. 22 (2008) 565–574.
[261] T. Ous, C. Arcoumanis, J. Mech. Eng. Sci. 221 (2007) 1067–1074.
[262] I. Fekrazad, T.L. Bergman, J. Heat Transf. 129 (2007) 1004–1013.
[263] J. Becker, V. Schulz, A. Wiegmann, J. Fuel Cell Sci. Technol. 5 (2008) 21006–21015.
[264] Y.W. Chen-Yang, T.F. Hung, J. Huang, F.L. Yang, J. Power Sources 173 (2007) 183–188.
[265] S. Voss, H. Kollmann, W. Kollmann, J. Power Sources 127 (2004) 93–97.
[266] V. Kamavaram, V. Veedu, A.M. Kannan, J. Power Sources 188 (2009) 51–56.
[267] R. Thiedmann, F. Fleischer, C. Hartnig, W. Lehnert, V. Schmidt, J. Electrochem. Soc. 155 (2008) B391–B399.
[268] E. Antolini, R.R. Passos, E.A. Ticianelli, J. Power Sources 109 (2002) 477–482.
[269] I. Han, S.H. Chan, S.P. Jiang, J. Power Sources 159 (2006) 1005–1014.
[270] A. Caillard, C. Charles, R. Boswell, P. Brault, C. Coutanceau, Appl. Phys. Lett. 90 (2007) 223119–223128.
[271] A. Caillard, C. Charles, R. Boswell, P. Brault, Nanotechnology 18 (2007) 305603–305612.
[272] T.H. Ko, Y.K. Liao, C.H. Liu, New Carbon Mater. 22 (2007) 97–101.
[273] J.M. Tang, M.E. Itkis, C. Wang, X. Wang, Y. Yan, R.C. Haddon, Micro. Nano. Lett. 1 (2006) 62–65.
[274] F.Y. Zhang, S.G. Advani, A.K. Prasad, J. Power Sources 176 (2008) 293–298.
[275] T.H. Ko, Y.K. Liao, C.H. Liu, Energy Fuels 22 (2008) 4092–4097.
[276] E. Sengul, S. Erkan, I. Eroglu, N. Bac, Chem. Eng. Commun. 196 (2009) 161–170.
[277] J.H. Lin, W.H. Chen, S.H. Su, Y.K. Liao, T.H. Ko, J. Power Sources 184 (2008) 38–43.
[278] H.F. Hung, J. Huang, H.J. Chuang, S.H. Bai, Y.J. Lai, Y.W. Chen-Yang, J. Power Sources 184 (2008) 165–171.
[279] Y.K. Liao, T.H. Ko, C.H. Liu, Energy Fuels 22 (2008) 3351–3354.
[280] A. Caillard, C. Charles, R. Boswell, P. Brault, J. Phys. D: Appl. Phys. 41 (2008) 185307.
[281] C.H. Liu, T.H. Ko, E.C. Chang, H.D. Lyu, Y.K. Liao, J. Power Sources 180 (2008) 276–282.
[282] C.H. Liu, T.H. Ko, Y.K. Liao, J. Power Sources 178 (2008) 80–85.
[283] A.M. Kannan, L. Munukutla, J. Power Sources 167 (2007) 330–335.
[284] E. Antolini, R.R. Passos, E.A. Ticianelli, J. Appl. Electrochem. 32 (2002) 383–388.
[285] S.E. Iyuke, A.B. Mohamad, A.A.H. Kadhum, W.R.W. Daud, C. Rachid, J. Power Sources 114 (2003) 195–202.
[286] H.S. Park, Y.H. Cho, C.R. Jung, J.H. Jang, Y.E. Sung, Electrochim. Acta 53 (2007) 763–767.
[287] S. Shimpalee, U. Beuscher, J.W. Van Zee, J. Power Sources 163 (2006) 480–489.
[288] J.H. Jang, W.M. Yan, C.C. Shih, J. Power Sources 161 (2006) 323–332.
[289] M. Coppo, N.P. Siegel, M.R. Von Spakovsky, J. Power Sources 159 (2006) 560–569.
[290] J.X. Wu, Q.Y. Liu, J. Fuel Cell Sci. Technol. 2 (2005) 20–28.
[291] G. Inoue, T. Yoshimoto, Y. Matsukuma, M. Minemoto, J. Power Sources 175 (2008) 145–158.
[292] W.C. Weng, W.M. Yan, H.Y. Li, X.D. Wang, J. Electrochem. Soc. 155 (2008) B877–B886.
[293] Z.Q. Zhang, W. Xia, X.X. Zhang, J. Li, J. Fuel Cell Sci. Technol. 5 (2008), 031007.1-031007.9.
[294] K.P. Adzakpa, K. Agbossou, Y. Dube, M. Dostie, M. Fournier, A. Poulin, IEEE Trans. Energy Convers. 23 (2008) 581–591.
[295] M. Secanell, K. Karan, A. Suleman, N. Djilali, J. Electrochem. Soc. 155 (2008) B125–B134.
[296] S.M. Chang, H.S. Chu, J. Power Sources 172 (2007) 790–798.
[297] A.A. Shah, G.S. Kim, W. Gervais, A. Young, K. Promislow, J. Li, S. Ye, J. Power Sources 160 (2006) 1251–1268.
[298] Q. Dong, M.M. Mench, S. Cleghorn, U. Beuscher, J. Electrochem. Soc. 152 (2005) A2114–A2122.
[299] S.M. Chang, H.S. Chu, J. Power Sources 161 (2006) 1161–1168.
[300] K. Tajiri, C.Y. Wang, Y. Tabuchi, Electrochim. Acta 53 (2008) 6337–6343.
[301] J.H. Lin, W.H. Chen, S.H. Su, Y.J. Su, T.H. Ko, Energy Fuels 22 (2008) 2533–2538.
[302] A.M. Kannan, S. Sadananda, D. Parker, L. Munukutla, J. Wetrz, J. Power Sources 178 (2008) 231–237.
[303] E. Gűlzow, M. Schulze, N. Wagner, T. Kaz, R. Reissner, G. Steinhilber, A. Schneider, J. Power Sources 86 (2000) 352–362.
[304] M. Uchida, Y. Aoyama, N. Eda, A. Ohta, J. Electrochem. Soc. 142 (1995) 463–468.
[305] Y.H. Pai, J.H. Ke, H.F. Huang, C.M. Lee, Z. Jyh-Myng, F.S. Shieu, J. Power Sources 161 (2006) 275–281.
[306] M.S. Saha, A.F. Gulla, R.J. Allen, S. Mukerjee, Electrochim. Acta 51 (2006) 4680–4692.
[307] A.F. Gulla, M.S. Saha, R.J. Allen, S. Mukerjee, J. Electrochem. Soc. 153 (2006) A366–A371.
[308] A.F. Gulla, M.S. Saha, R.J. Allen, S. Mukerjee, Electrochem. Solid State Lett. 8 (2005) A504–A508.
[309] W.M. Yan, C.Y. Hsueh, C.Y. Soong, F.L. Chen, C.H. Cheng, S.C. Mei, Int. J. Hydrogen Energy 32 (2007) 4452–4458.
[310] K. Fushinobu, D. Takahashi, K. Okazaki, J. Power Sources 158 (2006) 1240–1245.
[311] D. Yakisir, F. Mighri, M. Bousmina, J. Fuel Cell Sci. Technol. 5 (2008) 31008–31017.
[312] I. Furuya, N. Mineo, J. New Mater. Electrochem. Syst. 10 (2007) 205–208.
[313] X.L. Wang, H.M. Zhang, J.L. Zhang, H.F. Xu, B.L. Yi, Prog. Chem. 18 (2007) 507–513.